



OPEN ACCESS

EDITED BY

Assimina Antonarakou,
National and Kapodistrian University of
Athens, Greece

REVIEWED BY

Luca Basilone,
University of São Paulo, Brazil
Mumtaz Ali Khan,
Bahia University, Pakistan
Imad Mahmood Ghafor,
University of Sulaymaniyah, Iraq
Hamad Ur Rahim,
Pakistan Museum of Natural History, Pakistan

*CORRESPONDENCE

Xiucheng Tan,
✉ tanxiucheng70@163.com

RECEIVED 25 December 2024

ACCEPTED 19 March 2025

PUBLISHED 27 March 2025

CITATION

Yang M, Tan X, Xu F, Hao D, Zhao J, Li C,
Huang J and Li P (2025) Controlling factors
and evolution of reservoirs in continental rift
lacustrine carbonate factory: insight from the
cretaceous ITP-BVE formation in Brazil's
Santos Basin.

Front. Earth Sci. 13:1551406.

doi: 10.3389/feart.2025.1551406

COPYRIGHT

© 2025 Yang, Tan, Xu, Hao, Zhao, Li, Huang
and Li. This is an open-access article
distributed under the terms of the [Creative
Commons Attribution License \(CC BY\)](https://creativecommons.org/licenses/by/4.0/). The
use, distribution or reproduction in other
forums is permitted, provided the original
author(s) and the copyright owner(s) are
credited and that the original publication in
this journal is cited, in accordance with
accepted academic practice. No use,
distribution or reproduction is permitted
which does not comply with these terms.

Controlling factors and evolution of reservoirs in continental rift lacustrine carbonate factory: insight from the cretaceous ITP-BVE formation in Brazil's Santos Basin

Mengying Yang^{1,2}, Xiucheng Tan^{1,2*}, Fang Xu³, Duo Hao⁴,
Junfeng Zhao⁴, Chenqing Li³, Jixin Huang³ and Peijia Li^{1,2}

¹State Key Laboratory of Oil and Gas Reservoir Geology and Exploitation, Southwest Petroleum University, Chengdu, China, ²Division of Key Laboratory of Carbonate Reservoirs, China National Petroleum Corporation, Southwest Petroleum University, Chengdu, China, ³PetroChina Research Institute of Petroleum Exploration and Development, Beijing, China, ⁴China National Oil and Gas Exploration and Development Company Ltd., Beijing, China

The Cretaceous Itapema and Barra Velha Formations in Brazil's Santos Basin represent a rare giant rift lacustrine carbonate factory with considerable potential for oil and gas exploration. Through a comprehensive petrological and petrophysical analysis of field A in Santos Basin, this study clarifies the reservoir properties and distribution of this lacustrine carbonate facies and further investigates the controlling factors and differential evolution of lacustrine carbonate reservoirs. The main research results are as follows: (1) The Itapema Formation is characterized by bioclastic limestones that predominantly feature primary interparticle pores. As the alkalinity and salinity of the lake water gradually increased, the reservoir rocks of the Barra Velha Formation evolved into shrubstones and intraclastic limestones, with reservoir spaces comprising growth-framework pores and interparticle pores. (2) High-quality reservoirs are distributed regularly and cyclically below the exposure surfaces of high-frequency cycles. The quality of the reservoir exhibits an improvement from the bottom to the top of upward-shallowing sequences. These sequences, which are generally stacked vertically, enhance the heterogeneity of the reservoir. (3) Fluctuations in lake levels have facilitated the process of penecontemporaneous karstification, resulting in the formation of numerous dissolved pores and vugs. Generally, karstification enhances the quality of reservoirs; however, excessive karstification at the tops of cycles may result in the infilling of clay within breccias, consequently diminishing reservoir quality. (4) Multiple magmatism during rift evolution exert a dual control on reservoir space. Intense silicification can lead to the complete filling of pores and fractures with siliceous cement, thereby compromising reservoir spaces. However, rim-like siliceous cements formed during syn-depositional magmatism effectively isolate pore spaces, inhibiting material exchange during shallow burial. This process achieves a balance between dissolution and precipitation that ultimately preserves porosity. In general, reservoirs within the Itapema Formation exhibited a developmental trajectory that transitioned from superior primary porosity to karst-enhanced intraparticle

porosity, ultimately resulting in rim-like siliceous cements that preserved the pores. In contrast, the reservoirs of the Barra Velha Formation experienced a different evolutionary process, commencing with the differentiation of matrix porosity, which was subsequently increased by karstification. During the penecontemporaneous and burial stages, the pores infilled with silica and dolomite cements. This study presents a systematic analysis of the reservoir properties and diagenetic evolution of this set of lacustrine carbonate rocks. It contributes to the theoretical understanding of lacustrine carbonate deposition and provides valuable references for carbonate reservoir exploration in rift lake basins.

KEYWORDS

lacustrine, carbonate factory, reservoir properties, controlling factor, cretaceous, santos basin

1 Introduction

Carbonate factories refer to the environment where carbonate sediments are generated in large quantities. Schlager and other researchers have categorized marine carbonate factories based on the sources and environmental conditions of carbonate minerals (Schlager, 2003; Schlager, 2005; Reijmer, 2021). They have conducted comprehensive studies on various aspects, including petrological characteristics (Pomar and Hallock, 2008; Li et al., 2021), the evolution of sedimentary environments (Read, 1982; Read, 1985; Tucker et al., 1990; Li et al., 2015), reservoir properties (Moore and Wade, 2013; Li et al., 2023), and the mechanisms underlying reservoir formation (Xiao et al., 2016; Xiong et al., 2019). While the sedimentation processes and reservoir characteristics of lacustrine carbonates exhibit similarities to those of marine carbonates (Alonso-Zarza et al., 2020; Chinelatto et al., 2020), research focusing specifically on lacustrine carbonate factories remains limited. Lacustrine carbonate factories occur in various environments, including temperate-climate marl lakes in high latitudes (Murphy and Wilkinson, 1980), arid intermountain alkaline lakes (Chidsey et al., 2015), and subtropical rift lakes (Rebelo et al., 2021). It is generally acknowledged that the carbonate rocks formed in rift lakes tend to be relatively thin layers (Leleu and Hartley, 2010; Basilone et al., 2024), significantly smaller in scale compared to marine carbonate rocks (McArthur et al., 2013). As a result, substantial reserves of oil and gas associated with these rift lacustrine carbonate formations are considered to be quite rare on a global scale.

The Santos Basin is situated in the eastern maritime region of Brazil, specifically on the western flank of the South Atlantic Ocean. It is part of a series of passive continental margin basins that developed during the Mesozoic to Cenozoic epochs, coinciding with the rifting of West Gondwana and the subsequent formation of the South Atlantic (Aslanian et al., 2009; Torsvik et al., 2009; Moulin et al., 2010). Recent advancements in the exploration of carbonate rocks have resulted in the significant discovery of a substantial lacustrine carbonate reservoir from the rift period within Brazil's Santos Basin. This reservoir exhibits a thickness of up to 1 km and encompasses an area exceeding 12,000 square kilometers. Prior research conducted within the fields of paleontology (Poropat and Colin, 2012a; Poropat and Colin, 2012b; Pietzsch et al., 2018), sedimentology (Wright, 2012;

Costa De Oliveira et al., 2021) and geochemistry (Pietzsch et al., 2018; Mercedes-Martín et al., 2019; Mercedes-Martín et al., 2022) has substantiated the assertion that the carbonate rocks from the Cretaceous period functioned as a lacustrine carbonate factory.

The evolution of the continental rift system is characterized by terrestrial supplies (Basilone et al., 2017), volcanic activity (Wei et al., 2022), and the weathering of basalt (Shang et al., 2020), all of which contribute significant quantities of Ca^{2+} and Mg^{2+} . As a result, the continental rift system is favorable for the formation of saline-alkaline lake basins (Moore and Wade, 2013). At present, the pre-salt carbonate formations in the Santos Basin exhibit significant potential for exploration. Nonetheless, there are notable variations in reservoir quality between the Itapema and Barra Formations, characterized by considerable vertical heterogeneity. Understanding these variations and their origins is essential for guiding future exploration efforts. Given the intricate sedimentary and diagenetic conditions present in rift lake basins, a multitude of factors, including terrestrial input (Xiong et al., 2021), climatic variations (Xiao et al., 2021), precipitation and evaporation (Xiong et al., 2019), alterations in factory types (Li et al., 2021), synsedimentary volcanic activity (Lima and De Ros, 2019), and the protracted diagenetic evolution process (Carvalho et al., 2022), will significantly influence the differential development of reservoirs.

Therefore, this study conducts a comprehensive analysis of petrological and petrophysical data derived from the Itapema and Barra Velha Formations of field A, aiming to elucidate the types of reservoir rocks, characteristics of reservoir space, physical properties and distribution of the Cretaceous carbonate rocks in the Santos Basin. Furthermore, the study further elucidates the primary factors influencing reservoir development and explores the differential reservoir evolution of continental rift lacustrine carbonates, providing a reference case for future researches on lacustrine carbonate factories.

2 Geological background

The Santos Basin is located off the southeastern coast of Brazil, approximately at 30° S latitude (Figure 1A), and was formed during the Early Cretaceous, coinciding with the initial separation of the South American and African plates (Torsvik et al., 2009). The northeastern boundary of the basin is delineated by the Cabo

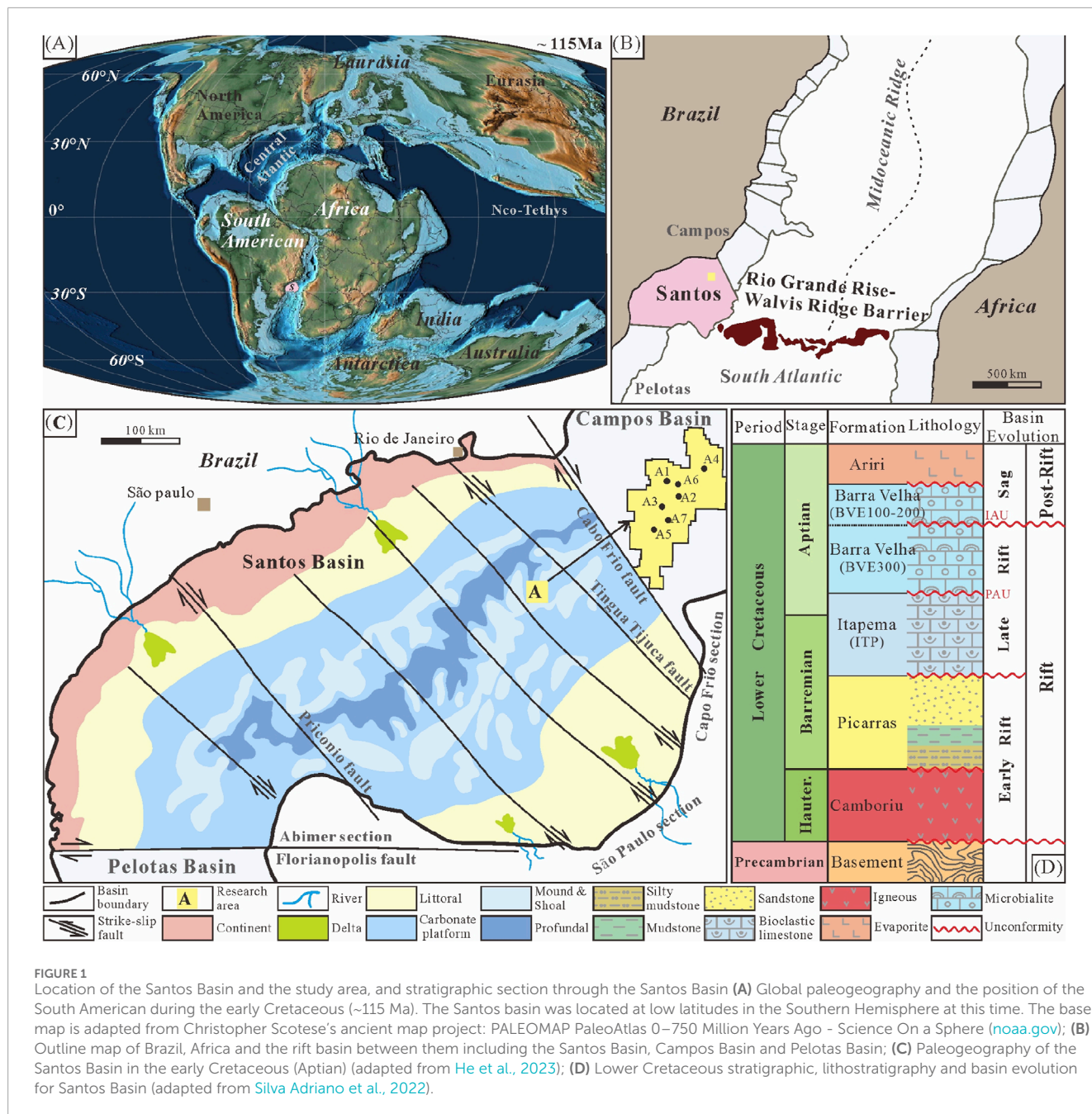


FIGURE 1 Location of the Santos Basin and the study area, and stratigraphic section through the Santos Basin (A) Global paleogeography and the position of the South American during the early Cretaceous (~115 Ma). The Santos basin was located at low latitudes in the Southern Hemisphere at this time. The base map is adapted from Christopher Scotese's ancient map project: PALEOMAP PaleoAtlas 0–750 Million Years Ago - Science On a Sphere (noaa.gov); (B) Outline map of Brazil, Africa and the rift basin between them including the Santos Basin, Campos Basin and Pelotas Basin; (C) Paleogeography of the Santos Basin in the early Cretaceous (Aptian) (adapted from He et al., 2023); (D) Lower Cretaceous stratigraphic, lithostratigraphy and basin evolution for Santos Basin (adapted from Silva Adriano et al., 2022).

Frio Fault, adjacent to the Campos Basin, while the southwestern boundary extends to the Florianópolis Fault, which adjoins the Pelotas Basin (Torsvik et al., 2009; Thompson et al., 2015). The southeastern side is characterized by the Rio Grande Rise and Walvis Ridge (O'Connor and Duncan, 1990), which were generated as a result of volcanic activity associated with rifting (Figure 1B). The basement fracture system of the Santos Basin controls multiple structural units that predominantly exhibit a northeast orientation, arranged sequentially from terrestrial to marine environments (Moreira et al., 2007). These structural units include the Western Sag, the Awu Uplift, the Central Sag, the Lusu Uplift, and the Eastern Sag (Shi et al., 2021). The field A is situated in the northern region of the Lusu Uplift.

The tectonic and sedimentary evolution of the Santos Basin can be categorized into three primary phases: Rift (Valanginian to Aptian), Post-rift (Aptian) and Drift (Albian to Holocene) (Moreira et al., 2007). During early syn-rift, the basin's crystalline basement, which consists of granite and gneiss, was unconformably overlain by basalt of the Camboriú Formation, with deposition occurring approximately between 134 and 122 Ma (Mizusaki et al., 1992). Overlying this volcanic rock sequence is the Picarras (PIC) Formation, which developed a fluvial-lacustrine sedimentary system characterized by sandstones, basaltic clasts and deep lacustrine shales.

During the late syn-rift phase, two distinct sets of lacustrine carbonate successions were deposited within the basin. The first

succession is Itapema (ITP) Formation, which comprises bioclastic grainstones, bioclastic rudstones, marlstone and dark mud shales (De Oliveira Nardi Leite et al., 2020; Thompson et al., 2015). The subsequent succession is the Barra Velha (BVE) Formation, which is unconformably located above the Itapema Formation. This unconformity also recognized in the Campos Basin as a regional long-term exposure surface, known as the Pre-Alagoas Unconformity (PAU) (Moreira et al., 2007). The rocks in the Barra Velha Formation include shrubstones, spherulitstones, intraclastic grainstones, mudstone and dolomite, as well as Mg-silicate clays containing spherulites and fine-to medium-grained dolomite (Wright, 2022). An additional unconformity within the Barra Velha Formation, known as the Intra-Alagoas Unconformity (IAU), delineates the transition between the syn-rift and sag phases (Buckley et al., 2015; Wright and Barnett, 2020). During this period, the lacustrine environment evolves from the interior to the periphery, transitioning from profundal to carbonate platform (microbialite and bioclastic limestone) and ultimately to littoral. Proximal to the land boundary, the formation of deltas and rivers occurs. The area of interest, designated as field A, is located within the carbonate platform (Figure 1C).

During the post-rift, the influx of seawater resulted in the termination of lacustrine carbonate deposition. The basin boundary's barrier effect, combined with evaporation processes, facilitated the formation of a marine evaporative lagoon. This environment led to the deposition of a substantial salt layer, reaching thicknesses of up to 2 km, within the central basin, which is a component of the extensive evaporite sequence of the Ariri Formation (Rodriguez et al., 2018).

By the end of the Early Cretaceous, the tectonic evolution of the basin entered drift phase and gradually transformed into passive continental margin (Moreira et al., 2007; Zhang et al., 2020).

3 Materials and methods

This study conducted a systematic observation and analysis of core samples from the Itapema and Barra Velha Formations obtained from seven wells in field A (#A1, #A2, #A3, #A4, #A5, #A6, #A7, Figure 1). The investigation encompassed approximately 350 m of core depth and around 1,000 sidewall core samples. By interpreting the core data, the study identified various rocks, reservoir spaces, sedimentary structures, and karstification features, while also developing lithological and structural profiles. All thin sections were impregnated with blue epoxy resin to enhance the visibility of porosity and stained with Alizarin Red S to distinguish between different carbonate minerals (e.g., calcite and dolomite). These thin sections were then described in detail using polarized and cathodoluminescence microscopy. Under reservoir pressure conditions, multiple sidewall core samples were tested for effective porosity and absolute permeability. All tests were conducted by Petrobras, and the detailed results of the petrophysical analysis are internal non-public data. The average porosity of different rock facies is calculated using the arithmetic mean, whereas the average permeability is determined using the geometric mean.

4 Results

4.1 Facies and characteristics of reservoir rocks

4.1.1 Bioclastic grainstone and rudstone

Bioclastic limestones are primarily composed of bivalves and ostracods (Figure 2A). The bivalves are frequently exhibit fragmentation as a result of wave action in lacustrine settings, characterized by a random orientation, favorable rounding, and sorting. The lengths of the shells may attain up to 10 mm, while their thicknesses generally surpass 0.5 mm. The observed characteristics indicate sediment deposition in a high-energy environment situated above the normal wave base of the lake. Some bivalve and ostracod shells are notably well-preserved, displaying distinct textures (Figure 2B). The particles exhibit moderate sorting and often horizontal stacking, which suggests deposition occurring in proximity to the wave base. This environment is conducive to the accumulation of bivalves *in situ* after death or their transportation over short distances by wave action. Bioclastic limestones can be further categorized according to grain size into two classifications: bioclastic grainstones, which have a grain size of less than 2 mm, and bioclastic rudstones, which possess a grain size exceeding 2 mm.

Micritic envelopes have been identified on the surfaces of shells (Figures 2B, C). Additionally, certain bioclasts have undergone recrystallization into substantial medium-grained calcite (Figures 2B–D, F, H).

4.1.2 Intraclastic grainstone and rudstone

The primary components of intraclastic limestone consist of fragments of reworked spherulitestone, shrubstone and laminated carbonates. The particles additionally comprise irregular siliceous grains (Figure 3). These particles demonstrate a moderate degree of rounding and sorting, characterized by normally grading (Figure 3A) or inverse grading (Figure 3B). The intraclast grain size varies between 0.02 cm and 4 cm (Figure 3C). Intraclastic limestones can be further categorized according to grain size into two classifications: intraclastic grainstones, which have a grain size of less than 2 mm, and intraclastic rudstones, which possess a grain size exceeding 2 mm. Intraclastic particles display point-line contact, with localized silicification of the grains (Figures 3F, G).

4.1.3 Shrubstone

Shrubstone is composed of fibrous-radial calcite (Figure 4A). It can be categorized into two distinct types based on the dimensions of its growth-framework: shrubby shrubstones, which have a single-cluster growth framework height of less than 2 cm, and arborescent shrubstones, characterized by a single-cluster growth framework height exceeding 2 cm. Shrubby shrubstones predominantly occur in stratified deposition, exhibiting clumped, low-relief domal structures (Figure 4A). In contrast, arborescent shrubstones are characterized by more prominent clustered domal structures (Figures 4B, C). The core often reveals an interbedded deposition of shrubstones alongside layered spherulitstones at the bottom, with an upward trend in the scale of the growth framework. Multiple clusters of growth frameworks exhibit a tacking growth

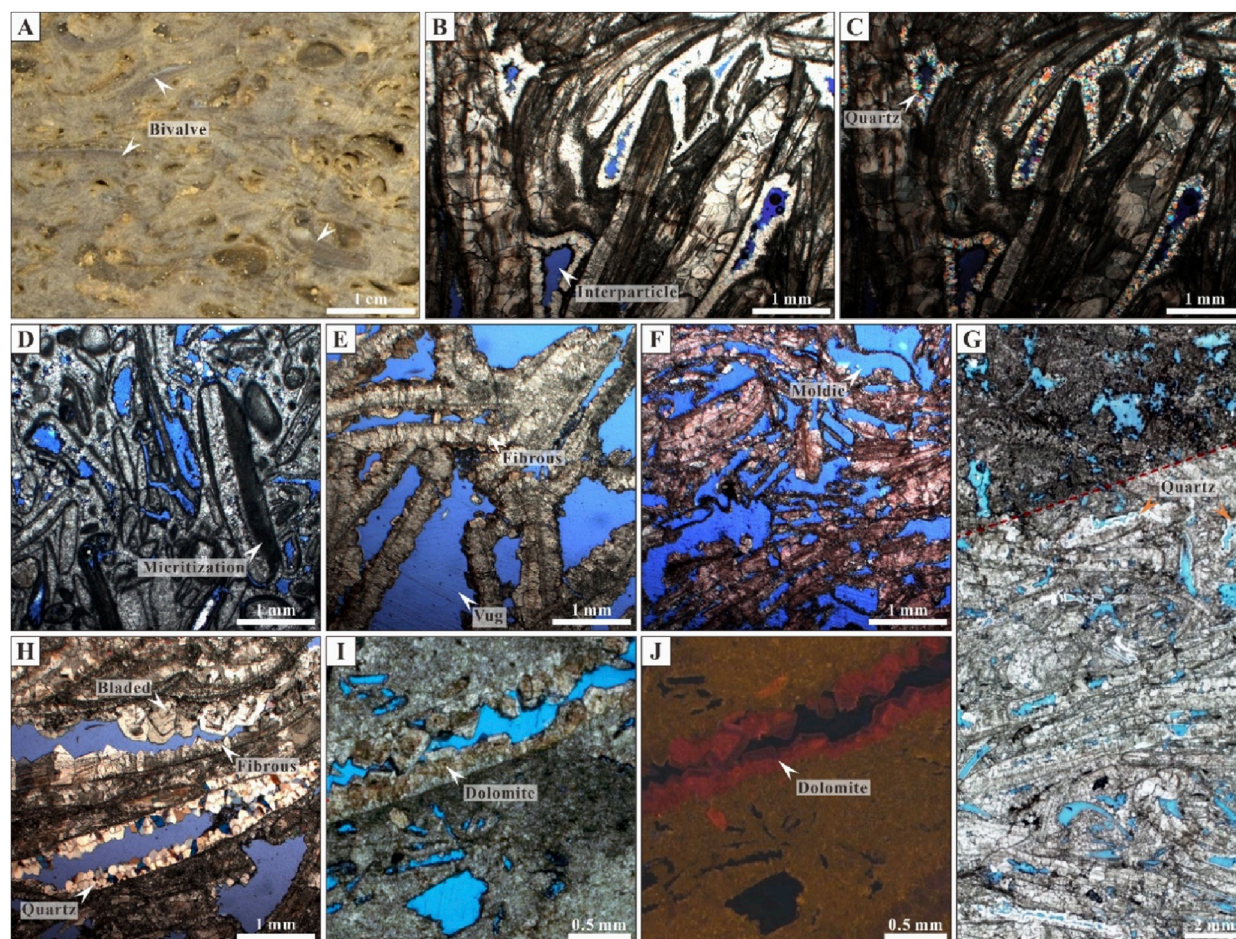


FIGURE 2 Petrographic features of bioclastic grainstone and rudstone **(A)** Bioclastic rudstone with fabric-selective dissolution vugs, #A2, 5,331.12 m, core; **(B)** Bioclastic rudstone, shell recrystallization, with siliceous rim-like cement and interparticle residual pores, #A2, 3,544.50 m; **(C)** Crossed polarized light image with the same field as B; **(D)** Bioclastic grainstone, with dark micritic envelope on shells, calcite cement infilling interparticle pores, #A1, 5,623.35 m; **(E)** Bioclastic rudstone, showing moldic pores and small vugs in shells, with fibrous calcite cements inside and outside shells, #A2, 5,340.55 m; **(F)** Bioclastic grainstone, with shell recrystallization and moldic pores, #A2, 5,379.70 m; **(G)** Bioclastic rudstone, showing moldic and interparticle dissolved pores, with silica cement in pores and intense dissolution at the top resembling brecciation, #A2, 5,338.25 m; **(H)** Bioclastic rudstone with moldic and interparticle dissolved pores, fibrous and bladed calcite cements, and silicified fringe cement, #A2, 5,373.30 m; **(I)** Packstone with residual moldic and interparticle dissolved pores infilled with medium-grained dolomite cement, #A2, 5,351.80 m; **(J)** Cathodoluminescence view of I, showing dolomite with weak red luminescence at the edges and intense red luminescence in the center (white arrows).

pattern, and during transitional evolutionary phases, spherulitic shrubstones may emerge (Figure 4B). When observed under cross-polarized light, the growth framework reveals a distinctive radiating extinction. The single-cluster growth frameworks typically feature a nucleus composed of peloids, which transitions into a shrubby morphology in the upper regions (Figures 4D, E). In certain areas, the growth framework has undergone silicification, which obscures its original structural characteristics (Figures 4A, C, D, F).

4.1.4 Spherulitestone

Spherulitestones are characterized by aggregates of calcite that are spherical to subspherical in shape. Some spherulites exhibit preferential growth patterns along specific orientations, leading to the formation of asymmetrical structures with diameters that

range from 0.1 to 2 mm. When observed under cross-polarized light, these spherulites exhibit distinctive radiating extinction (Figure 5). Spherulitestones can be found in either laminated (Figure 5A) or massive forms (Figure 5C). They can be further classified based on the proportions of shrubs and spherulites into shrubby spherulitestone, shrubby spherulitestone with mud, muddy spherulitestone, and spherulitic mudstone. Typically, at the base of sedimentary cycles, spherulitestones are associated with micritic limestones or micritic spherulitestones in a rhythmic depositional (Figure 5A). As one moves upward in the facies sequence, there is an observed increase in spherulite size accompanied by a decrease in argillaceous content (Figure 5B), which may lead to the transformation of spherulitestones into shrubby spherulitestones (Figure 5C). The contact between spherulites ranges from point to suspended. Locally, spherulites may undergo recrystallization

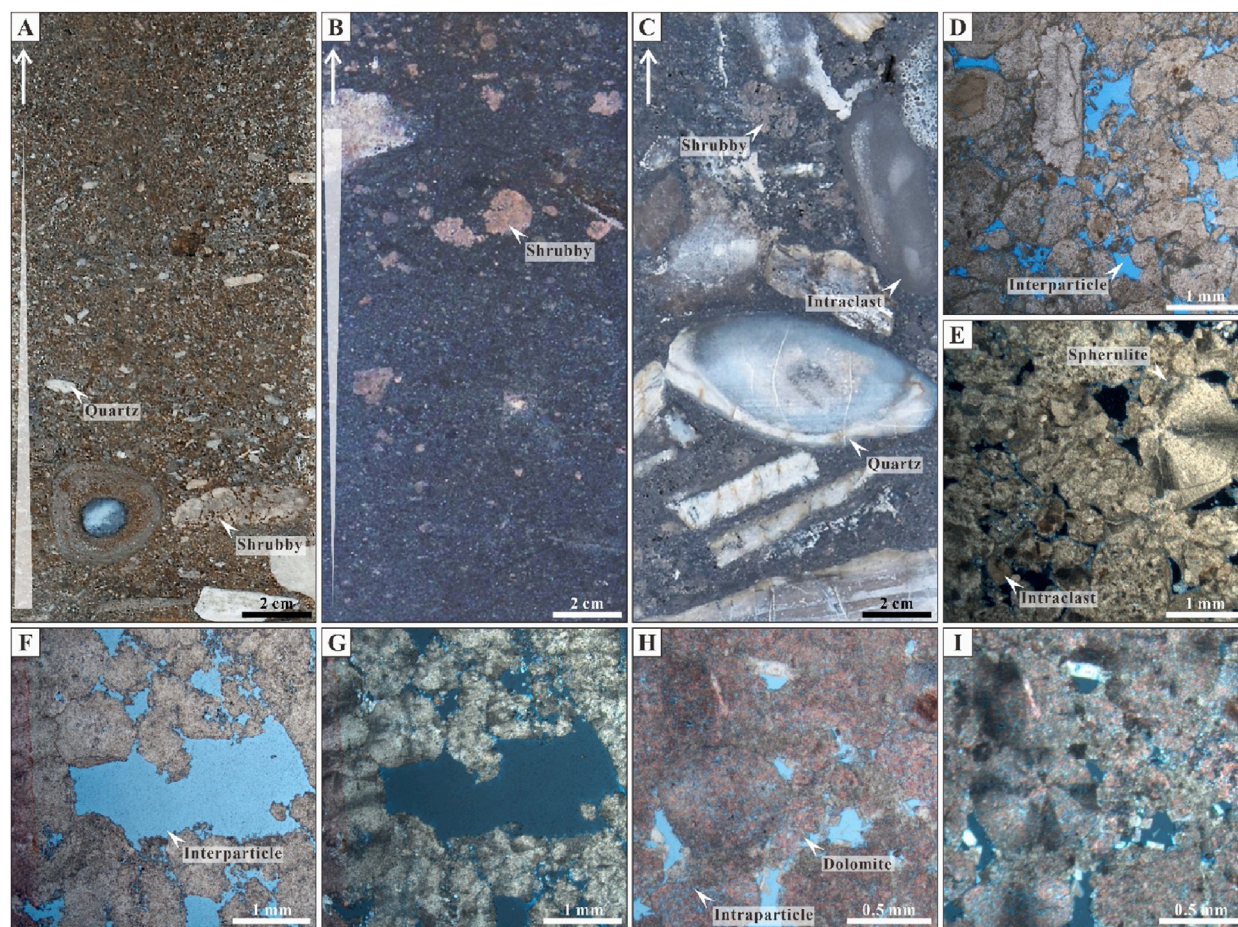


FIGURE 3
 Photographs of intraclastic grainstone and rudstone in this study. (A) Intraclastic rudstone with normal grading and interparticle pores, #A1, 5,548.40 m, core; (B) Intraclastic rudstone with inverse grading, #A3, 5,472.25 m, core; (C) with interparticle pores, #A3, 5,489.40 m, core; (D) Intraclastic grainstone with point-line contact among grains, showing interparticle and intraparticle dissolved pores, #A6, 5,582.35 m; (E) Intraclastic grainstone with spherulite fragments and interparticle pores; (F) Intraclastic grainstone showing interparticle dissolved pores, with local small dissolved vugs and partial silicification of grains, #A3, 5,502.95 m; (G) Crossed polarized light image with the same field as F; (H) Intraclastic grainstone with recrystallized grains, fine-grained dolomite, and anhydrite infilling interparticle pores, with residual interparticle and intraparticle dissolved pores, #A3, 5,460.80 m; (I) Crossed polarized light image with the same field as (H)

(Figure 5G) or dolomitization, resulting in the presence of residual grain ghosts (Figure 5J).

4.1.5 Packstone

Packstones are classified as grain-supported facies characterized by the presence of mud and micrite. They consist of over 50% reworked materials, which include fragments of shrubs, peloids, spherulite, and bioclasts (Figures 2I, 5A). The grains within these facies are generally rounded to sub-rounded and exhibit varying degrees of sorting, ranging from poorly to well-sorted. At the macroscale, packstones are generally characterized by their massive or laminated structures, which are interspersed with layers rich in mud that consist of carbonate minerals or Mg-clays.

4.1.6 Wackstone

Wackstones are classified as mud-supported facies characterized by the presence of over 10% ostracod bioclasts and

reworked materials, which encompass fragments of shrubs, peloids, and spherulites. At the macroscale, these facies exhibit a matrix-supported structure that may be massive or display plane-parallel lamination (Figures 6A, B). At the microscale, they are composed of a finely laminated muddy matrix (Figure 6C). The predominant grain types within these facies are fragments of spherulites and bioclasts.

4.1.7 Mudstone

At the macroscale, mudstones exhibit hues ranging from gray to dark brown. These facies are characterized by fine lamination and plane-parallel bedding, as well as rhythmic interbedding with marlstones (Figures 6D, F). At the microscale, the composition is predominantly micrite and mud, constituting over 90% of the material (Figure 6E), with minor occurrences of bivalves, spherulites, and other grains dispersed within the matrix.

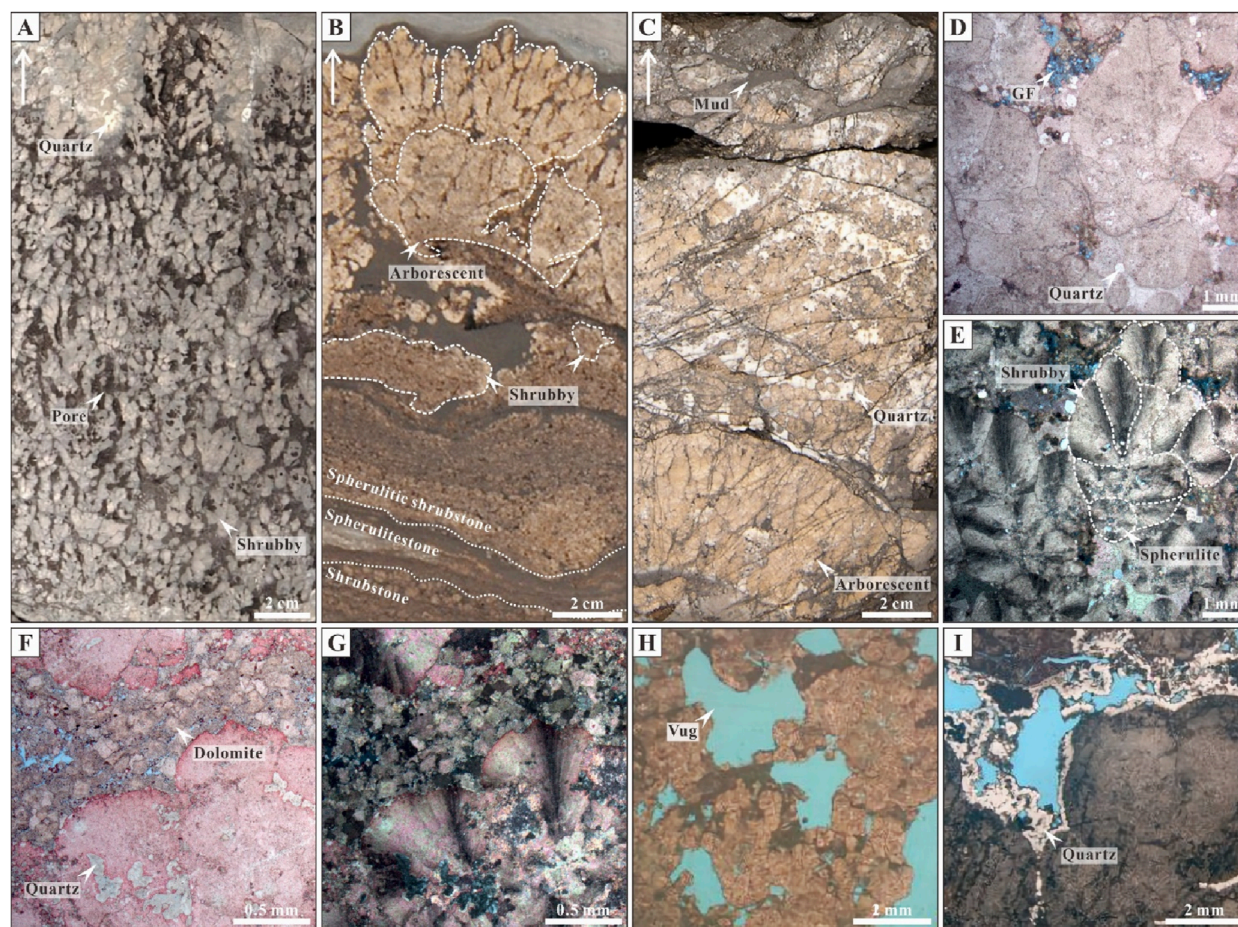


FIGURE 4
 Photographs of shrubstone in this study. (A) Shrunken shrubstone, single-cluster growth-framework diameter <2 cm, with growth-framework pores (GF) infilled by siliceous cement, #A4, 5,231.35 m, core; (B) Shrunken shrubstone, lower section exhibits interbedded arborecent shrubstone and spherulitestone, evolving upward into arborecent shrubstone. Single-cluster growth-framework diameter >2 cm, with frameworks infilled by argillaceous material and framework fragments, #A6, 5,483.45 m; (C) Arborecent shrubstone, upper framework exhibits brecciation, with insoluble residual dark argillaceous material and siliceous cement, #A4, 5,234.50 m; (D) Shrunken shrubstone, framework dissolved pores infilled by siliceous cement and insoluble dark residues, #A3, 5,523.60 m; (E) Crossed polarized light image with the same field as D; (F) Shrunken shrubstone, partial silicification of growth-frameworks, with interstitial dark insoluble material and fine- to medium-grained dolomite crystals, some showing etched crystal edges, #A3, 5,504.70 m; (G) Crossed polarized light image with the same field as F; (H) Shrunken shrubstone: small vugs, locally infilled by dark argillaceous material, #A5, 5,555.00 m; (I) Shrunken shrubstone, small vugs with rim-like siliceous cement, #A4, 5,228.15 m.

4.2 Reservoir properties

4.2.1 Types and characteristics of reservoir spaces

The reservoir spaces demonstrate diverse types and rich combinations, and can be categorized as pore-to vug-type reservoirs. The primary pore types identified include interparticle pores, intercrystalline pores, and growth-framework pores. In contrast, the secondary pore types consist of intraparticle dissolved pores, moldic pores, interparticle dissolved pores, growth-framework dissolved pores, intercrystalline dissolved pores, and micropores between infillings. Additionally, small dissolved caves are commonly observed within the examined region, alongside sporadic fractures, as detailed in Table 1.

Interparticle pores, growth-framework pores and vugs are primarily found between bioclasts (Figures 2B, C), intraclasts

(Figures 3D, E), shrubs (Figure 4I), and spherulites (Figure 5H), serving as high-quality reservoir spaces. These pores exhibit a size range of 0.1–2 mm and are frequently partially infilled by calcite or siliceous cements. Furthermore, clay introduced during the initial phase of lacustrine transgression is likely to infiltrate the growth-framework pores.

Intraparticle dissolved pores form due to the fabric-selective dissolution of shell fragments (Figures 2D, G), intraclasts (Figures 3H, I), and spherulites (Figure 5F) under the influence of meteoric freshwater during the penecontemporaneous stage. These features predominantly occur within bioclastic limestones, intraclastic limestones, and spherulitestones. Locally, these pores are frequently infilled with cements, display irregular geometries, and exhibit variability in size. Furthermore, these pores tend to be relatively isolated, demonstrating limited connectivity.

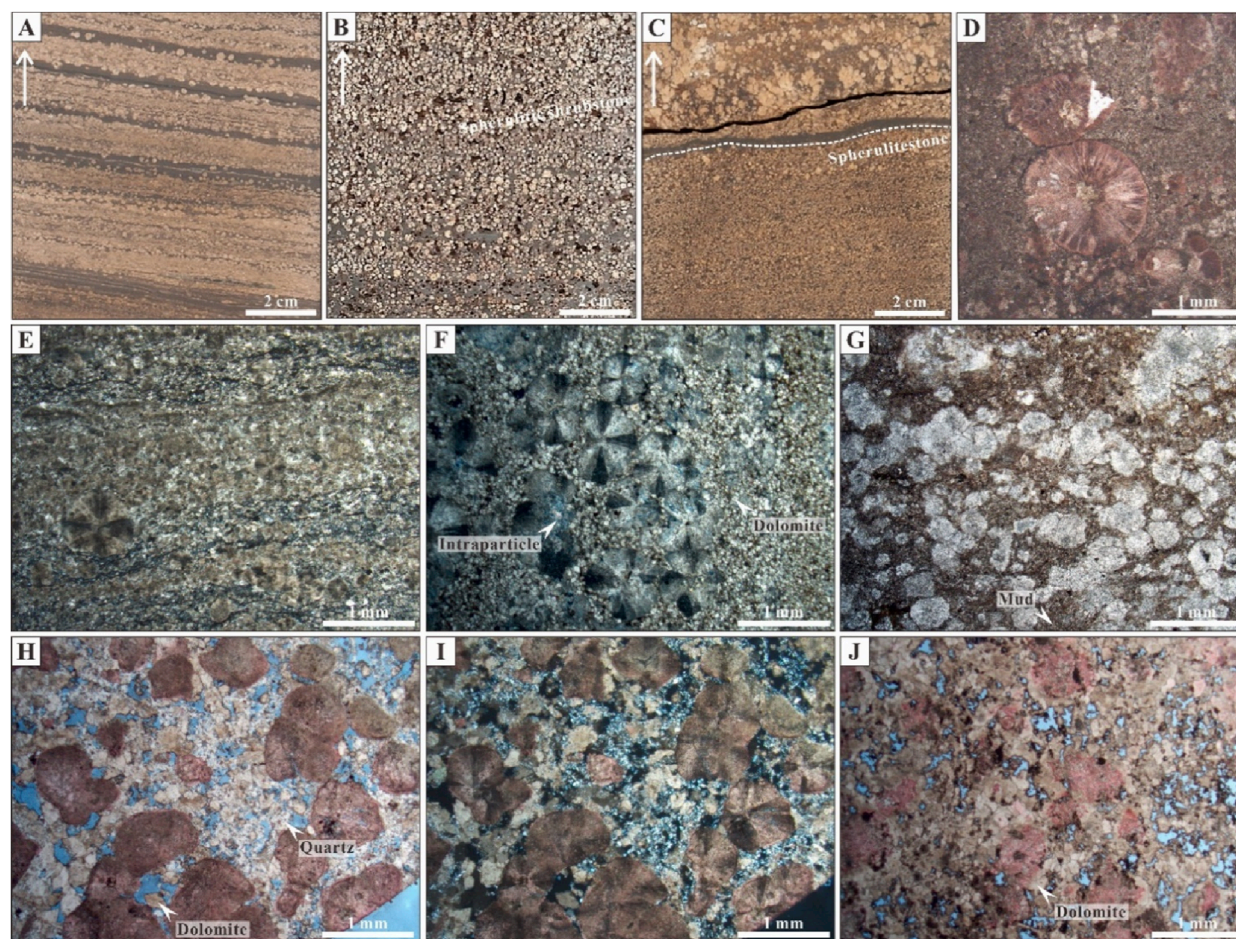


FIGURE 5 Photographs of spherulitestone in this study. **(A)** Spherulitestone, rhythmically interbedded with mudstones and packstones, #A6, 5,575.85 m, core; **(B)** Spherulitestone, upward increase in grain size and reduction in interstitial argillaceous content, with development of interparticle pores, #A7, 5,342.60 m, core; **(C)** Spherulitestone, upward increase in grain size, evolving into spherulitic shrubstone; #A6, 5,474.65 m, core; **(D)** Spherulitestone, intraparticle fibrous radiating structure with diameters up to 1.5 mm, interparticle spaces infilled with calcite cement, #A3, 5,467.45 m; **(E)** Spherulitestone, spherulites <0.5 mm in diameter, #A3, 5,448.35 m; **(F)** Spherulitestone with fine-grained dolomite, #A6, 5,575.80 m; **(G)** Muddy spherulitestone, recrystallized spherulites, #A3, 5,450.45 m; **(H)** Spherulitestone, intraparticle pores infilled with fine- to medium-grained dolomite and minor siliceous cement, #A6, 5,392.20 m; **(I)** Crossed polarized light image with the same field as H; **(J)** Calcareous spherulitic dolostone, calcareous spherulites replaced by dolomite, showing grain ghosts and residual intercrystalline dissolved pores, #A6, 5,396.5 m.

Moldic pores are formed through the complete dissolution of the shells of bioclasts, leaving only the micritic envelopes to form the pore space (Figures 2E–G). These pores retain the external morphology of the original particles and are primarily found within the Itapema Formation. The pores may be either unfilled or partially infilled with calcite cements, with some pore diameters exceeding 2 mm. In general, these pores are relatively isolated, but the dissolution of the micritic envelopes may enhance pore connectivity.

Interparticle dissolved pores, growth-framework dissolved pores and caverns are generated through non-fabric selective dissolution within the meteoric freshwater seepage zone. Diagenetic fluids migrate through the pre-existing interparticle pores (Figure 2F), growth-framework pores (Figures 4D, E, I) and high-permeability layers, leading to the dissolution of certain matrix or cements. This process results in the formation of irregular, embayed

pore margins and significant variation in pore size. These pores have the potential to interconnect with other pore types, thereby establishing a well-connected network of reservoir spaces.

Intercrystalline dissolved pores are frequently observed in shrubstones (Figures 2F, G), calcareous spherulitic dolomite (Figures 5H–J), and mudstone (Figure 6E). On one hand, shubby frameworks or spherulites are frequently infilled with fine- to medium-grained dolomite, resulting in the formation of intercrystalline pores. On the other hand, spherulitestones undergoes a process of dolomitization, which leads to the development of intercrystalline pores, that subsequently transform into intercrystalline dissolved pores through the dissolution of meteoric freshwater. These pores exhibit irregular shapes, with diameters typically measuring less than 0.5 mm, exhibiting moderate connectivity, and limited development in the study area.

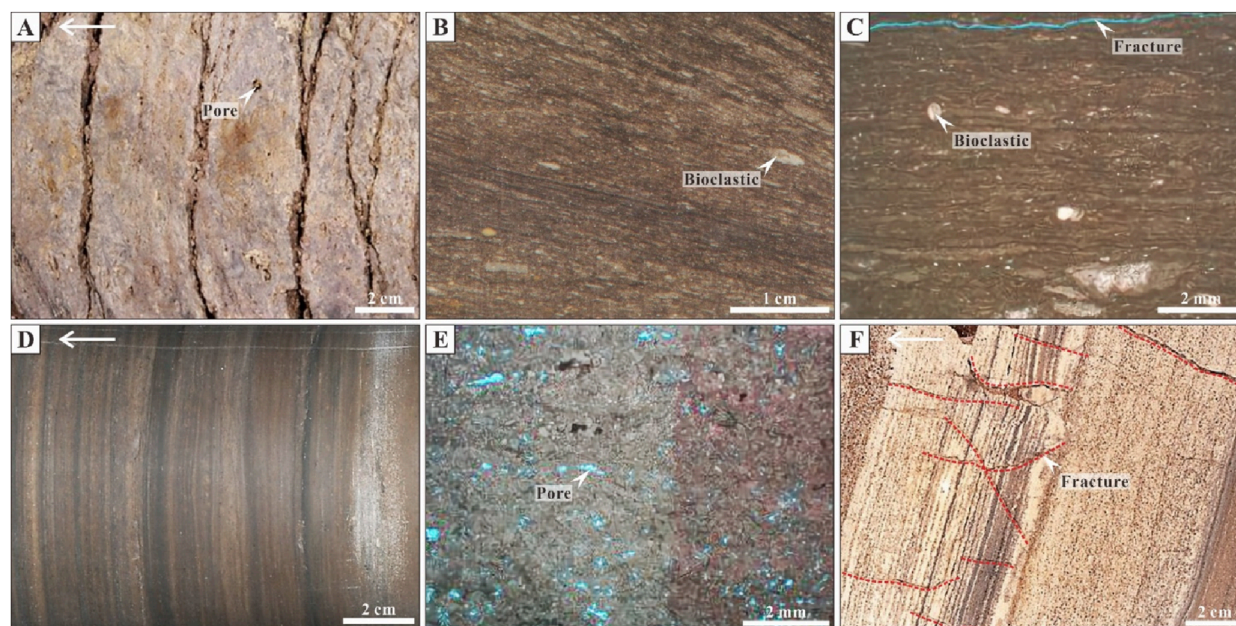


FIGURE 6
Photographs of mudstone and packstone in this study. (A) Wackstone, #A2, 5,327.40 m, core; (B) Wackstone, #A3, 5,848.00 m, core-sidewall; (C) Wackstone with fracture, #A5, 5,706.00 m; (D) Laminated mudstone, rhythmically interbedded with dark marlstones, #A1, 5,564.45 m; (E) Mudstone with intercrystalline dissolved pores, #A2, 5,293.00 m; (F) Laminated mudstone with fracture, #A7, 5,343.75 m.

Micropores between infillings are a consequence of residual insoluble materials, such as vadose silt, present within karst-modified pores, vugs, and channels (Figure 2G). These micropores represent a typical reservoir space type found in karst systems.

The Itapema and Barra Velha Formations within the examined region display porous and vuggy reservoir spaces (Figures 3F,G; Figure 4H), some of which are infilled with silica or calcite, with pore diameters typically exceeding 2 mm. These reservoir spaces mainly formed in bioclastic limestones, intraclastic limestones, and shrubstones.

Fractures encompass both dissolved fractures and those associated with dissolution-related breakage (Figure 4C; Figures 6C, F). Both types play significant roles in enhancing pore connectivity and improving local permeability. Nevertheless, fractures are typically underdeveloped within the examined region, predominantly occurring in low-energy mudstones or reservoir rocks that exhibit diminished density due to dissolution processes. These fractures arise under the pressure exerted by overlying strata.

4.2.2 Porosity and permeability characteristics of reservoir rocks

The Itapema and Barra Velha Formations exhibit generally favorable reservoir rock properties. Porosity ranges from 0% to 30% (average $12.3\% \pm 5.3\%$), with porosity between 5% and 20% accounting for 91.4% of the samples. Permeability varies between 0.01 mD and 4,200 mD, averaging 4.9 mD, with 62.3% of the samples having permeability between 0.1 mD and 100 mD (Figure 7A).

Among the four reservoir rock types, bioclastic limestones have the most favorable properties, followed by shrubstones and intraclastic limestones (Figure 7). The porosity of bioclastic limestone ranges from 3.5% to 30% (average $13.3\% \pm 5.2\%$), with 34.7% of samples having porosity exceeding 15%. Permeability ranges from 0 mD to 4,170 mD, averaging 19.9 mD, with 68.4% of samples having permeability exceeding 10 mD. In contrast, spherulitstones exhibit relatively poor properties, with 25.7% of samples having porosity below 5%, and 62.4% having permeability less than 1 mD. Overall, the properties of reservoir rocks in the studied area display strong heterogeneity. Reservoir rocks in the Itapema Formation show high porosity and permeability, while those in the Barra Velha Formation are characterized primarily by medium-to-high porosity and high permeability or medium porosity and medium-to-low permeability.

4.2.3 Distribution characteristics of single-well reservoir properties

In the Itapema Formation, bioclastic grainstone, bioclastic rudstone, and packstones found in the middle to upper sections of the sedimentary cycles demonstrate favorable reservoir qualities, with higher porosity and permeability correlating to larger bioclastic grain sizes (Figure 8). In the Barra Velha Formation, intraclastic grainstone, intraclastic rudstone, and shrubstones located in the middle to upper sections of the cycles exhibit relatively favorable reservoir qualities. Intraclastic limestones are noted for their high porosity and permeability ($\phi > 15\%$, $K > 100$ mD), while shrubstones present medium porosity coupled with either low permeability or medium porosity with high permeability. The breccia at the top of depositional cycles, along with mudstones, packstones,

TABLE 1 Reservoir space types of Itapema and Barra Velha Formation

Types of reservoir space		Main reservoir rock types	Development frequency
Primary pores	Interparticle pores	Bioclastic grainstones, bioclastic rudstones, intraclastic grainstones, intraclastic rudstones, spherulitestones, packstones	High
	Growth-framework pores	Shrubby shrubstones, arborescent shrubstones, spherulitic shrubstones	High
	vug	Bioclastic grainstones, bioclastic rudstones, intraclastic grainstones, intraclastic rudstones, packstones	Medium
Secondary Pores	Interparticle dissolved pores	Bioclastic grainstones, bioclastic rudstones, intraclastic grainstones, intraclastic rudstones, spherulitestones, packstones	High
	Growth-Framework dissolved Pores	Shrubby shrubstones, arborescent shrubstones, spherulitic shrubstones	High
	Intraparticle dissolved pores	Intraclastic grainstones, intraclastic rudstones, spherulitestones	Medium
	Moldic pores	Bioclastic grainstones, bioclastic rudstones, packstones	Medium
	Intercrystalline dissolved pores	Shrubby shrubstones, arborescent shrubstones, calcareous spherulitic dolomite, spherulitestones with fine- to medium-grained dolomite	Low
	Micropores between infillings	Karstificated rocks	Medium
	Caverns	Bioclastic grainstones, bioclastic rudstones, intraclastic grainstones, intraclastic rudstones, shrubby shrubstones, arborescent shrubstones	Medium
	Dissolved fractures and dissolution-related breakage fractures	wackstones, packstones	Low

and spherulitestones in the middle to lower part of depositional cycles, typically display poor reservoir properties, characterized by porosity around 5% and permeability below 1 mD. However, locally sediments deposited low-energy environments can exhibit enhanced reservoir properties, with significantly higher porosity and permeability, whereas sediments from high-energy may present porosity below 5%.

In well A6, the Itapema Formation is characterized by reservoir rocks consisting of bioclastic grainstones and rudstones, whereas the Barra Velha Formation is primarily composed of intraclastic grainstones. The cumulative reservoir thicknesses for these formations are 7.63 m and 9.08 m, respectively, representing 38.15% and 45.40% of the total well section. Overall, well A6 exhibits advantageous reservoir properties, with a greater cumulative reservoir thickness correlating with an increased frequency and thickness of grainstones and rudstones. In well A7, the Barra Velha Formation is predominantly composed of spherulites, shrubstones, and spherulitic mudstones. These reservoirs are larger in scale and exhibit good properties, with

a cumulative thickness of 15.12 m, accounting for 75.58% of the well section.

The Itapema Formation demonstrates marginally superior reservoir properties compared to the Barra Velha Formation. High quality reservoirs within high-energy sediments are distributed regularly and cyclically in the middle to upper parts of sedimentary cycles. Increased cumulative reservoir thickness and enhanced properties are associated with larger accumulations of high-energy sediments. In contrast, low-energy sediments found in the middle to lower sections of these cycles typically exhibit poor reservoir qualities. Overall, the reservoir properties observed at individual wells display significant heterogeneity.

5 Discussion

Vertical heterogeneity in reservoir properties has long been a central topic within the field of carbonate reservoir research. In recent years, a multitude of studies have investigated the

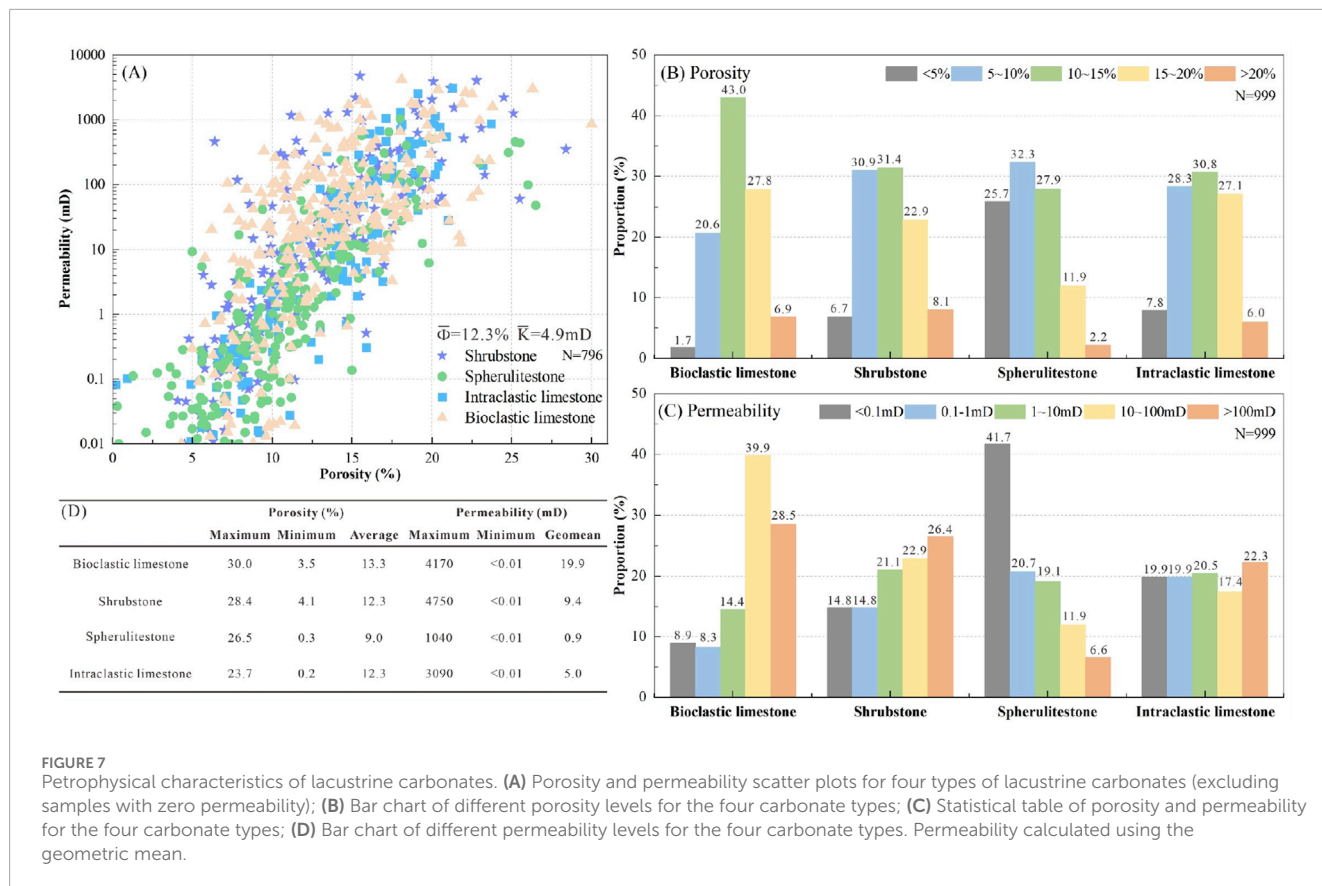


FIGURE 7 Petrophysical characteristics of lacustrine carbonates. (A) Porosity and permeability scatter plots for four types of lacustrine carbonates (excluding samples with zero permeability); (B) Bar chart of different porosity levels for the four carbonate types; (C) Statistical table of porosity and permeability for the four carbonate types; (D) Bar chart of different permeability levels for the four carbonate types. Permeability calculated using the geometric mean.

primary factors influencing this heterogeneity, considering aspects such as the reservoir rock types (Mehrabi et al., 2019; Zhao et al., 2019; Ye et al., 2021; Ghafor, 2022; Ghafor and Najaflo, 2022), favorable diagenetic conditions (Saller et al., 2016; Zhong et al., 2019; Xiong et al., 2019; Shah et al., 2021) and the conditions conducive to preservation (Mehrabi et al., 2016; Xiong et al., 2020a).

5.1 The influence of lacustrine environments on reservoir rock types

During the initial phase of rift evolution, the Picarras Formation developed deltas, where significant amounts of terrigenous clasts, transported by rivers systems, deposited within the narrow and profound lake (Scotchman et al., 2010). This influx of material led to a decrease in calcium carbonate saturation levels in the lake and inhibiting the development of lacustrine carbonate factories (Li et al., 2021).

During the late phase of rift evolution, the basin underwent further extension, resulting in a broad and shallow morphology (Einsele, 2000; Pietzsch et al., 2020). During this period, rising lake levels (Costa De Oliveira et al., 2021), coupled with the Awu Uplift obstructing the influx of terrigenous clasts from the east (Chen, 2022), facilitated the development of lacustrine carbonate factories during the period of deposition of the Itapema Formation (Figure 9). Within this environment, mollusks, particularly bivalves, thrived on stable basement. Fluctuations in paleoclimate influenced

the periodic variations in lake levels (Gomes et al., 2020), but the overall trend of rising lake level provided sufficient accommodation space. Smaller bivalves accumulated on the micritic substrate, resulting in the deposition of packstones containing a small amount of interparticle pores (Figure 9-Typ1). Larger bivalves were fragmented by the action of lake waves and subsequently accumulated in significant quantities, resulting in the formation of Bioclastic grainstone and rudstone characterized by numerous cavities (Figure 9-Typ2). Additionally, the high permeability layers within the high-energy shoals are relatively thick (Figure 8). The facies observed in the Itapema Formation exhibit a degree of simplicity, predominantly indicating variations in the composition and dimensions of bivalves in response to differing hydrodynamic conditions.

The deposition of the Barra Velha Formation was influenced by significant volcanic activity and hydrothermal contributions occurring during the Early Cretaceous Barremian to Aptian stages (Keller, 2008). This geological context, coupled with heightened evaporation rates within the lacustrine basin (Farias et al., 2019; Pietzsch et al., 2020), resulted in the development of highly alkaline and hypersaline lakes characterized by elevated concentrations of Ca, Mg, SiO₂(aq) and HCO₃²⁻ (Figure 9) (Yuretich and Cerling, 1983). These changes in water chemistry caused the mass mortality of bivalves (Pietzsch et al., 2018), ultimately prompting changes in the facies of the Barra Velha formation. In this highly alkaline and hypersaline environment, calcite attained a state of supersaturation, which promoted the development of spherulites with fibrous radial and polycrystalline structures internally (Wright and Barnett,

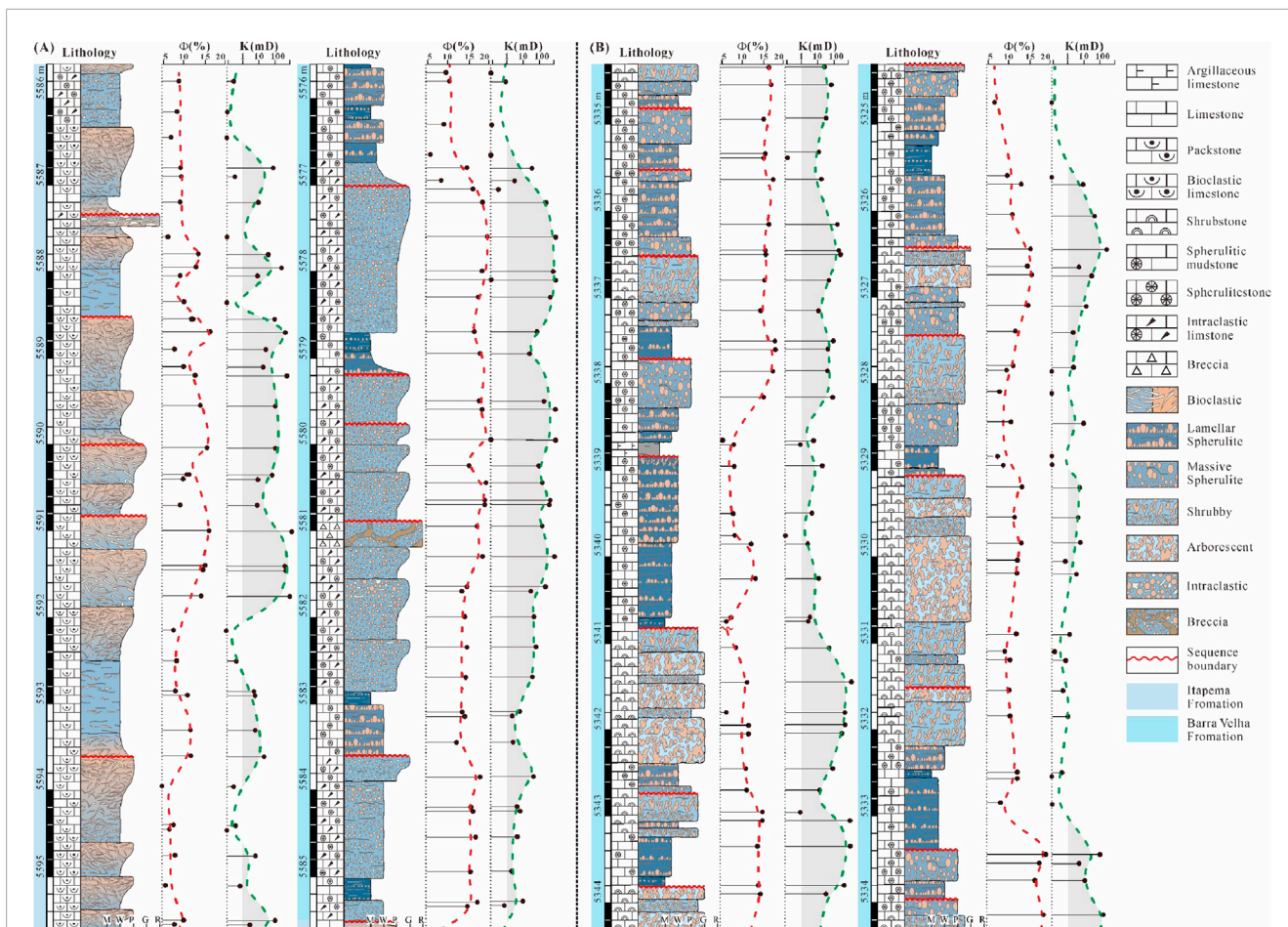


FIGURE 8 Lithostratigraphic columns and petrophysical properties of two cores in this study. (A) #A6, 5,595.30–5,575.80 m; (B) #A7, 5,344.15–5,324.65 m; Gray shadows indicate K > 1 mD, showing the reservoirs.

2015; Mercedes-Martín et al., 2019; Pietzsch et al., 2022). This has evolved into spherulitstones with interparticle pores (Figure 9-Typ4). However, the majority of these pores are infilled with Mg-silicate clays (Figure 9-Typ3). As the influence of terrigenous materials decreased, the content of Mg-silicate clays diminished. Concurrently, evaporation and concentration processes persisted, leading to an increase in pH levels (Gomes et al., 2020). As a result, spherulitstones progressively transformed into shrubstones and reservoir spaces is transformed into growth-framework pores (Figure 9-Typ6). The alterations observed in the reservoir rocks are influenced not solely by variations in the chemical properties of the water, but are also governed by the hydrodynamic conditions. The shallowing of lake water led to significant hydrodynamic activity, which resulted in the fragmentation of spherulitstones, shrubstones, and consolidated limestone. This fragmentation subsequently contributed to the accumulation of intraclastic limestones characterized by a high density of interparticle pores (Figure 9-Type 5).

During the post-rift depression phase, intense evaporation significantly increased the salinity of the lake (Farias et al., 2019), ultimately leading to the collapse of the carbonate factory and the deposition of thick evaporites (Figure 9).

As rifting continued, the influx of seawater into the basin during the Albian stage facilitated the revival of the carbonate factory, transitioning it into a marine carbonate factory (Modica and Brush, 2004).

In summary, the chemical properties of lake water drove the variations in the facies of lacustrine carbonate factory and controlled the differences in reservoir rock types.

5.2 High frequency cycles restrict the vertical distribution of reservoir characteristics

The reservoir properties in the studied area exhibit significant vertical heterogeneity (Figure 8), which is a critical element affecting and limiting exploration and development of the pre-salt formations in the Santos Basin (Shang et al., 2020; Jia et al., 2021; He et al., 2023). The facies sequences observed in wells demonstrate pronounced high-frequency stacking characteristics, which are intricately linked to the development of reservoirs. This research considers the depositional cycles of the Itapema and Barra Velha Formations as essential units for reservoir analysis, investigating

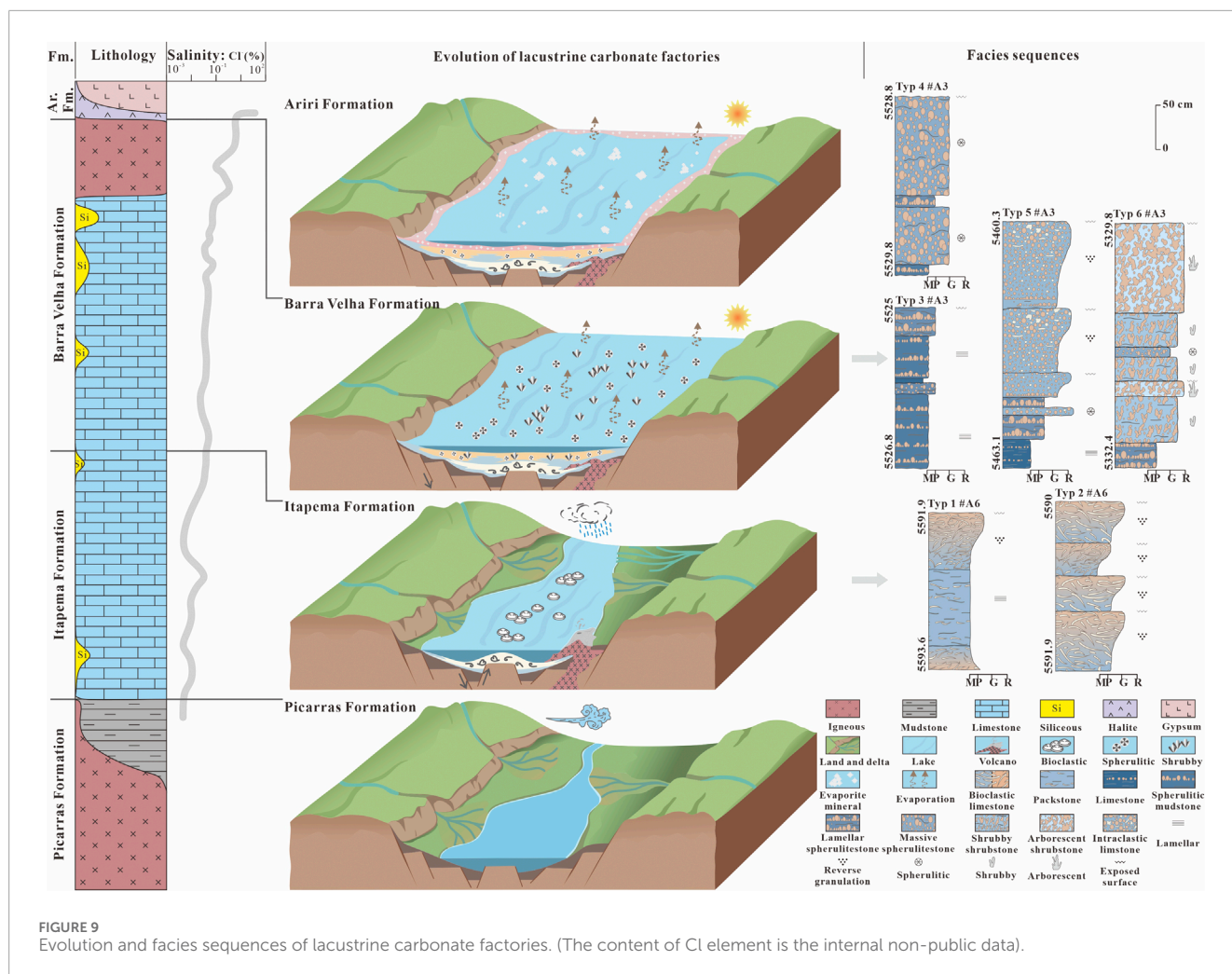


FIGURE 9 Evolution and facies sequences of lacustrine carbonate factories. (The content of Cl element is the internal non-public data).

the critical factors that affect the vertical heterogeneity of reservoir properties.

5.2.1 Facies sequences and reservoir properties of the itapema formation

Variations in hydrodynamic conditions have resulted in the development of distinct types of facies sequences. The lithological succession comprising mudstone, wackstone, and packstone with moderate reservoir quality developed in a low-energy environment (Figure 8) has smaller interparticle pore diameters. During the lake transgression period, the bottom of the cycle consists of mudstone with relatively poor reservoir properties. Above it, bioclastics are suspended in the micrite matrix, with localized development of pores. In the late stage of lake regression, the interparticle pores of small shells are infilled with a large amount of mud. Conversely, in the highland regions characterized by greater hydrodynamic energy, a lithological succession emerges that exhibits enhanced reservoir properties, which encompasses wackstone, packstone, bioclastic grainstone, and bioclastic rudstone (Figure 10A). From the base to the apex, the concentration of bioclastics within the single cycle exhibits an increase, accompanied by an enlargement in particle size. This phenomenon facilitates the formation of numerous

interparticle pores and cavities, thereby enhancing the reservoir quality. Consequently, within the upward shallowing sequence, there exists a strong correlation between the vertical distribution of reservoir rocks and their reservoir quality, as influenced by the facies sequence and the cyclical fluctuations of lake levels (Figures 8–10). The vertical stacking of multiple cycles leads to the alternating development of dense layers, low-permeability layers, and high-permeability layers.

Using well A2 as a case study, the interval ranging from 5,378.50 to 5,369.60 m is characterized by eight distinct and analogous high-frequency cycles (S1 – S8) (Figure 10A). Each of these cycles is comprised of wackstone, packstone, and limbioclastic grainstone. The individual cycles from S1 to S3 exhibit a relatively modest thickness, ranging from approximately 0.2–0.5 m. The total reservoir thickness characterized by porosity greater than 10% is less than 1 m. This phenomenon can be attributed to the rapid fluctuations in lake levels, which limited the available accommodation space and resulted in reduced energy within the water. Consequently, this led to the formation of thinner bioclastic limestone and smaller bioclastic particles during the regressive phase. Notably, the fractures that developed during this period significantly enhanced permeability, often exceeding 100

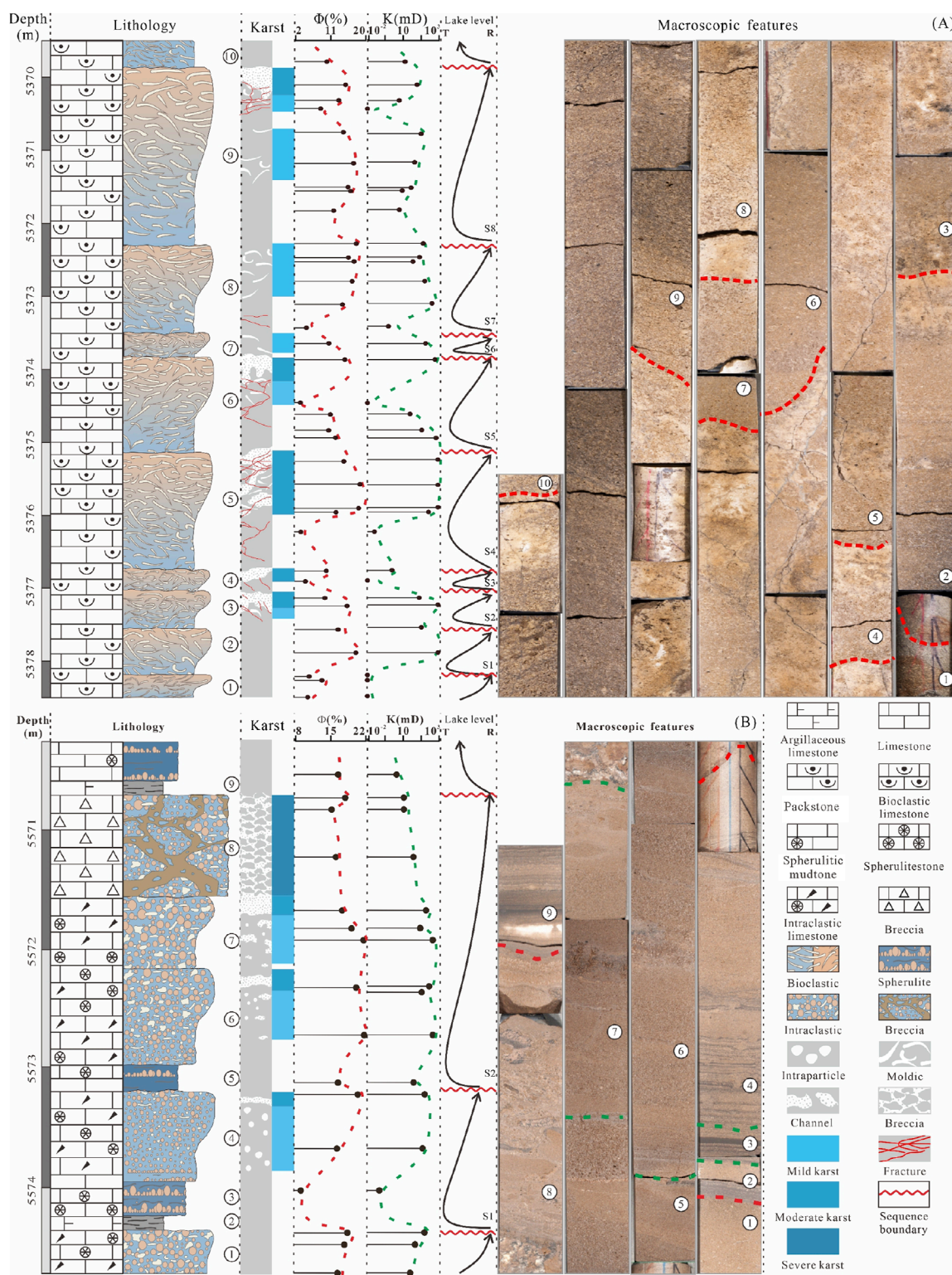


FIGURE 10 Petrophysical properties in high frequency facies sequences. (A) #A2, 5,378.50~5,369.60 m; (B) #A6, 5,574.95~5,570.05 m.

mD. In comparison, cycles S4 to S8 exhibit increased individual thicknesses, ranging from approximately 1.2–2.3 m, with reservoir thicknesses exhibiting over 10% porosity reaching up to 1.5 m within

a single cycle. This observation indicates that, under conditions characterized by adequate accommodation space and heightened hydrodynamic energy, the presence of mud between particles

diminished and the scale of shoal increased. As a result, the reservoir thickness associated with high porosity and high permeability has also improved (Figure 10A).

5.2.2 Facies sequences and reservoir properties of the Barra Velha formation

The transformation in the nature of the lacustrine carbonate factory controlled the changes in facies sequences in the Barra Velha Formation, thereby constraining the vertical heterogeneity of the reservoirs. This is mainly reflected in the following three aspects: (1) Mudstone often develops in the low-energy environment at the bottom of the facies sequence, which has poor reservoir quality. Concurrently, the growth-framework pores and interparticle pores located in the middle to lower sections of the cycle are frequently infilled by mud, argillaceous, and Mg-silicate clays, which leads to a reduction in reservoir porosity (Figures 5F–H). Among them, Mg-silicate clays is a typical product of alkaline lake system, which has been extensively documented in various regions of the Santos Basin and Campos Basin (Herlinger et al., 2017; Tosca and Wright, 2018; Gomes et al., 2020). (2) As the salinity of water at the uppermost layer of the facies sequence increases, the shrubstones transition from a shrubby form to an arborescent form (Basso et al., 2021). This transformation leads to an expansion of the primary growth-framework pore sizes. As a result, there is a progressive increase in both porosity and permeability from the base to the apex of the sequence. (3) The succession of spherulitstones, intraclastic limestones and shrubstones within upward-shallowing cycle controls the vertical distribution of reservoir spaces and reservoir quality.

Utilizing wells A7 and A6 as case studies, it is observed that Well A7 exhibits superior reservoir quality at the uppermost section of the cycle (Figure 8B). This is characterized by facies stacking pattern that progresses from mudstone, to spherulitic mudstone, followed by spherulitstone, and lastly culminating in shrubstone. The mudstone and spherulitic mudstone located at the base of the cycle exhibit suboptimal reservoir properties or are inadequately developed. An increase in the concentration of spherules leads to the gradual formation of interparticle pores. However, the layers with high porosity remain relatively thin. As interparticle pores progressively transition into growth-framework pores, there is a marked improvement in reservoir properties, with porosity attaining a peak of 18% and a reservoir thickness of approximately 1 m.

In well A6, the interval ranging from 5,574.95 to 5,570.05 m is characterized by two distinct facies sequences. The observed facies stacking pattern progresses from mudstone, to spherulitstone, followed by intraclastic grainstone. The intraclastic shoals within the lower S1 exhibit a thickness of less than 1 m and are characterized by a smaller scale. The porosity at the base of the laminated spherulitstones is approximately 8%, which increases to 20% in the upper sections. In contrast, the upper S2 is marked by multiple overlapping shoals, where porosity can reach up to 22% and thickness can extend to 1.5 m (Figure 10B). At the top of this sequence, breccias are formed, leading to a significant reduction in porosity. Statistical analyses suggest that intraclastic limestones demonstrate superior reservoir quality (Figure 7). Therefore, the facies sequence of spherulitstones and intraclastic limestone is recognized as the highest-quality reservoir unit in the Barra Velha Formation.

The vertical heterogeneity observed in the reservoirs of the Itapema and Barra Velha formations frequently demonstrates notable cyclicity. This pronounced heterogeneity can be primarily attributed to the alternating arrangement of high and low-quality reservoir layers, which arise from facies sequences and their vertical stacking (Saller et al., 1999; Mehrabi et al., 2019; Zhao et al., 2019).

5.3 Penecontemporaneous karstification enhances reservoir quality

In addition to the presence of a substantial quantity of high-quality primary porosity, the area under investigation also demonstrates a considerable variety of reservoir space types that have been formed as a result of dissolution processes (Figures 2–6, 11). Karstification, recognized as a significant diagenetic process in the development of high-quality carbonate reservoirs, has been the subject of considerable scholarly investigation (Saller et al., 1999; Xiao et al., 2016; Zhong et al., 2019; Xiong et al., 2019). The karstification processes occurring during the penecontemporaneous and supergene stages are the dissolution of carbonate minerals through the action of weakly acidic fluids (Grimes, 2006). These fluids are generated from low mineralization meteoric freshwater and the hydrolysis of carbonates.

In the investigated region, karstification within the carbonate rocks of the Itapema and Barra Velha formations are predominantly exhibited through the development of various types of pores. These pore types encompass interparticle dissolved pores (Figure 2G), intraparticle dissolved pores (Figure 3H; Figure 4F), moldic pores (Figures 2E, F; Figure 11A), channels (Figures 2F,G; Figures 11B–E), and breccia (Figures 11F, G). The variations among these pore forms can be primarily attributed to the duration of alteration by karstic fluids (Saller et al., 1999; Xiong et al., 2022). The alternating interplay of karst processes of differing intensities within the vertical dimension facilitates the formation of karstification sequences (Xie et al., 2020).

At the base of the facies cycle, primary pores are predominantly present, which progressively transition into interparticle dissolved pores as one moves upward, accompanied by fabric-selective dissolution in certain particles. Towards the upper portion of the facies cycle, exposure surfaces are frequently formed, characterized by vertically oriented channels or chaotically arranged karst breccias located beneath these exposure surfaces. The vertical stacking of multiple karstification sequences results in a recurrent alternating pattern of weak and strong dissolved carbonate (Figure 10). The fabric-selective dissolution of intraparticle pores and moldic pores is a characteristic feature of penecontemporaneous karstification. Consequently, it is posited that the karstification process transpired at an early stage with the observable dissolution predominantly driven by the fluctuations in lake surface. The factors influencing fluctuations in lake levels may not align with those affecting sea-level changes. Rather, they are more likely associated with the consistent climatic variations that occur during the sedimentary processes (Andrews and Hartley, 2015). The research conducted by Gomes et al. (2020) illustrates that variations in climate significantly affect the influx of terrigenous riverine contributions and the rates of evaporation from lake water. These interrelated factors play a crucial role in influencing fluctuations in lake levels and contribute to the development of facies sequences associated with microbialites.

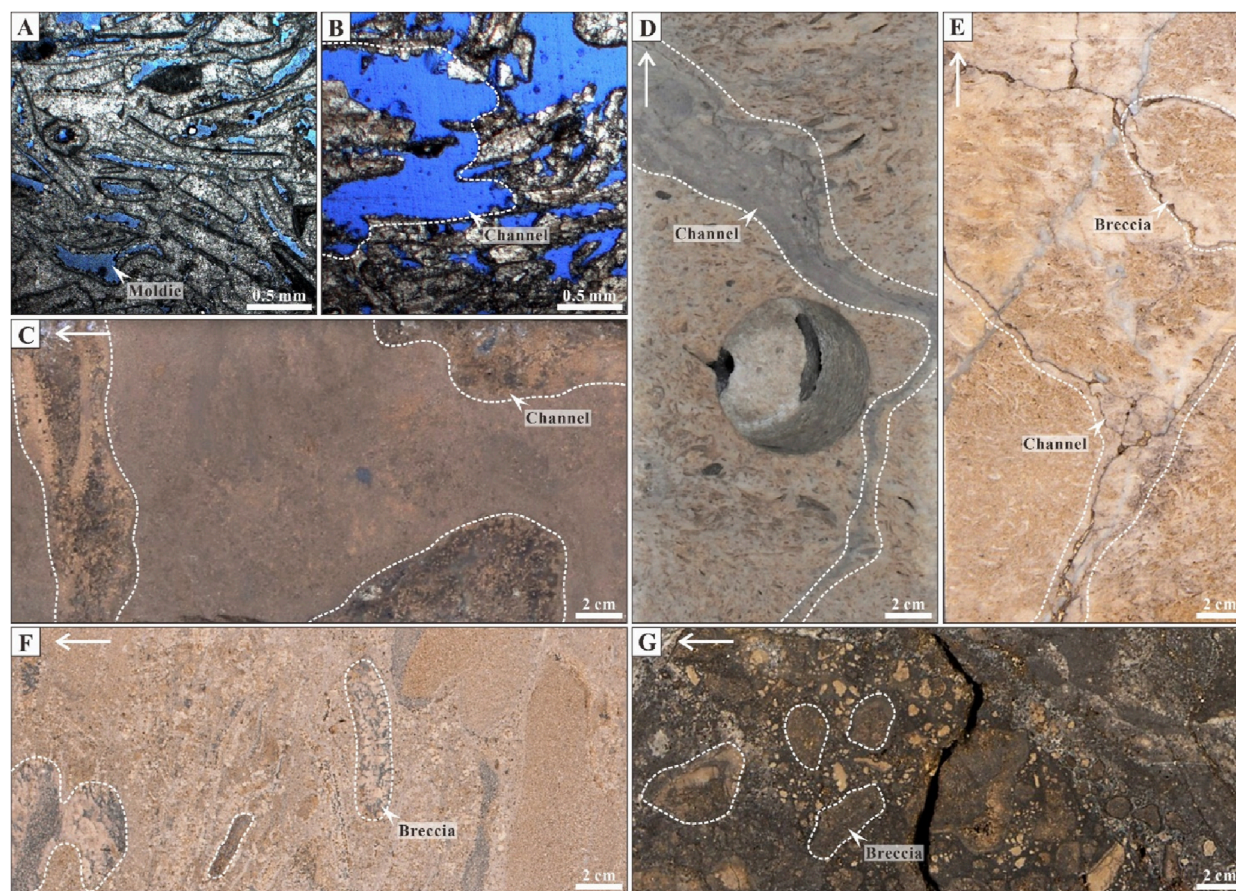


FIGURE 11

Photographs of penecontemporaneous karstification features in this study. (A) Bioclastic limestone with moldic pores, #A1, 5,629 m; (B) Bioclastic limestone showing dissolution of shell fragments and connection of interparticle pores, forming channels, #A2, 5,379.7 m; (C) Spherulitestone showing dissolution range enlarged, #A3, 5,529.8 m; (D) Bioclastic limestones with a small channel infilled with dark mud and detached bedrock fragments, #A1, 5,615.65 m; (E) Bioclastic limestone featuring channels containing breccias and dissolution-related breakage fractures, #A2, 52,275.1 m; (F) Breccia, #A6, 5,570.65 m; (G) Breccia with dark mud and fractured bedrock infilling the karst system, #A4, 5,238.8 m.

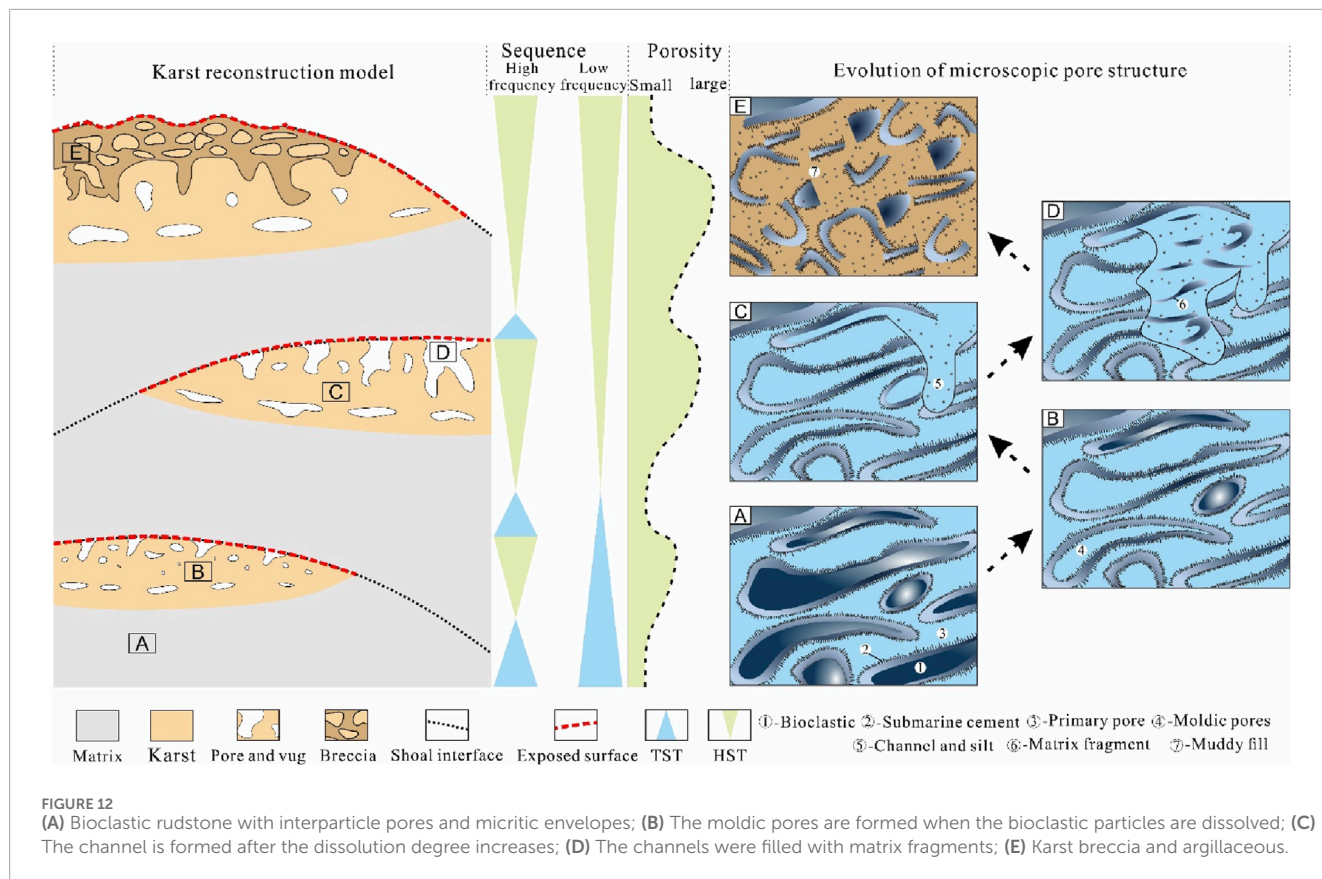
Given the widespread development of dissolution-modified reservoirs in the carbonate rocks, it is essential to conduct a more thorough investigation into the relationship between penecontemporaneous karstification processes and reservoir distribution (Figure 12). First, karstification processes improve or creates new types of reservoir space (Figure 11). The process of karstification enhances the reservoir properties in the upper section of the facies cycle, primarily due to the creation of numerous dissolution cavities. Secondly, fluctuations in the intensity of karstification processes significantly affect the vertical distribution of reservoir properties within a single facies sequence. For example, the permeability of the channels developed by moderate karstification processes (Figures 10A–S2; Figures 4, 5) is significantly greater than that of intraparticle pores resulting from mild karstification processes (Figures 10A–S6–8). This phenomenon can be attributed to the fact that karst processes enhance reservoir quality by loosening the matrix (Xiong Y. et al., 2023; Yang et al., 2024). In the later stages, the compaction of the overlying strata may lead to the formation of network-like

fractures, resulting in the development of a high-permeability layer (Figures 10A–S4; Figure 11E).

Karstification serves as a significant contributor to the formation of high-quality reservoirs. However, its effects are not universally beneficial. The escalation of karst intensity results in the collapse of the loosened bedrock characterized by dissolved cavities, thereby compromising the pore structure. The process of karstification results in the formation of disordered deposits of karst breccia at the uppermost layers of the cycles, accompanied by interstitial spaces between breccia infilled with vadose silt (Figure 12E). Consequently, this leads to a marked decline in the quality of the reservoir (Figures 10B–S2).

5.4 The reformation of reservoir properties by volcanic activity

During the rift evolution of the Santos Basin, magmatic activity occurred in multiple stages (Keller, 2008). The influx of magma and hydrothermal fluids into the lake environment



caused widespread silicification within the investigated region, with significant heterogeneity in intensity. Typically, silicification is notably more pronounced in proximity to intrusive igneous rocks. Observations from thin sections identify two principal characteristics of silicification: cementation and metasomatism. The siliceous minerals identified include quartz and chalcedony (Shang et al., 2020), with quartz crystals exhibiting a range of morphologies and structures, such as subhedral microcrystalline, medium-crystalline radial columnar, and coarse-crystalline cluster. Siliceous cementation typically occurs uniformly along the growth-framework or bioclastic surfaces, resulting in the formation of isopachous rim-like fibrous (Figures 4H, I; Figures 13E–G) and may either completely or partially infilling pores and fractures. When fractures develop within high-matrix-porosity reservoir rocks, silica-rich fluids tend to infiltrate the matrix pores, resulting in cementation and replacement. In some cases, features indicative of quartz replacement can be observed, including spherulites, growth-frameworks, and bioclasts.

Silicification not only obscured the original sedimentary characteristics but also significantly impacted reservoir properties during the shallow burial stage (Lima and De Ros, 2019; Xiong L. et al., 2023). During the period of deposition of the Itapema and Barra Velha Formations, intermittent influxes of basaltic lava flows into the lake, along with the weathering and leaching of basalt from the Camboriu Formation above the lake level, which contributed substantial quantities of dissolved Si, Ca, and Mg to the lake water (Szatmari and Milani, 2016). As the concentration of silica in pore fluids gradually

increased, microcrystalline quartz or chalcedony (Figure 13D) formed rapidly under favorable physicochemical conditions, leading to the consumption of pore spaces or the replacement of spherulites, growth-frameworks, and bioclasts (Lima et al., 2020). Furthermore, quartz exhibited a tendency to precipitate preferentially along the margins of pores, resulting in the formation of rim-like cement. This phenomenon often obstructed narrow pore throats, thereby isolating pore spaces and consequently diminishing permeability.

In the studied area, the homogenization temperatures of fluid inclusions in cluster-like quartz are abnormally high (Shang et al., 2020), indicating a strong correlation between silicification processes and hydrothermal activity. Additionally, areas characterized by intense hydrothermal silicification are closely associated with the distribution of diabase. Radiometric dating using the ⁴⁰Ar/³⁹Ar method indicates that the diabase at the top of the Barra Velha Formation originated during the Late Cretaceous drift stage, which aligns with the burial period of the carbonate rocks (Cheng et al., 2019). This evidence implies that following the intrusion of diabase, magmatic hydrothermal fluids migrated along fault zones through the carbonate strata, causing localized intense silicification, as evidenced by the complete filling of residual pores with cluster-like quartz. Furthermore, hydrothermal activity triggered by volcanic eruptions during the period of deposition of carbonate may also have led to the infilling of residual pores with siliceous cements. A large number of isolated pores surrounded by rim-like siliceous cements are observed in the studied area. The preservation of these isolated

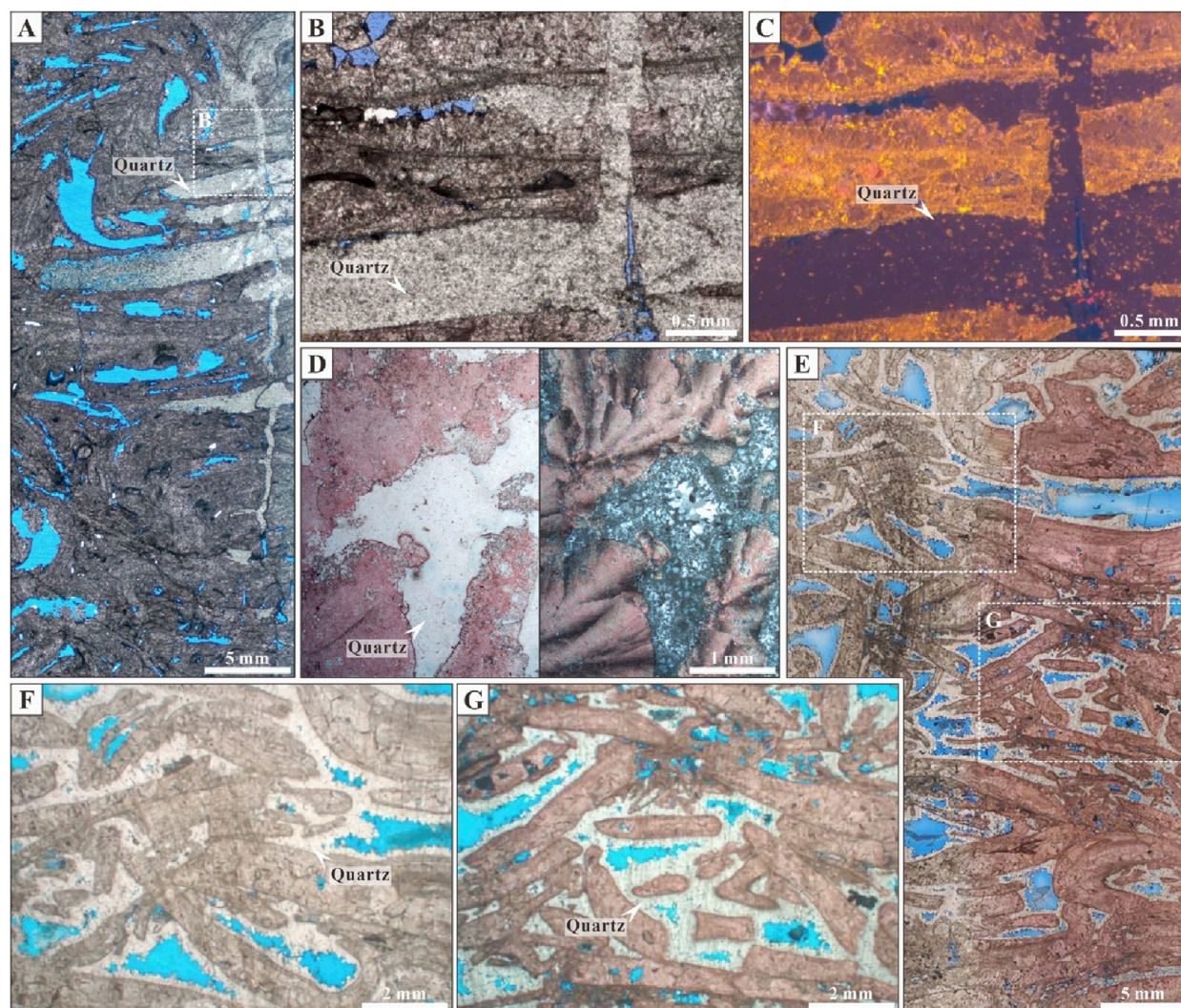


FIGURE 13
 Photographs of siliceous cement in this study. (A) Bioclastic rudstone showing moldic pores and small dissolution fractures infilled with siliceous cement, $\Phi = 14.4\%$, $K = 111.3$ mD, #A2, 5,361.65 m; (B) Magnified view of area in A; (C) Cathodoluminescence image of area in B, showing siliceous cement emitting low-intensity purple luminescence; (D) Arborescent shrubstones (-,+), with siliceous cement infilling pores and replacing the framework, #A3, 5,504.70 m; (E) Bioclastic rudstones with rim-like siliceous cement, $\Phi = 9.3\%$, $K = 0.96$ mD, #A2, 5,361.65 m; (F) and (G) Magnified views of area in E.

pores is attributed to the suppression of material exchange between pores during the shallow burial phase, achieving a dissolution-precipitation equilibrium (Xiong et al., 2020b; Wu et al., 2022) and thereby preventing excessive siliceous cementation within the pores.

Compared to bioclastic limestones, siliceous bioclastic limestones exhibits a reduction in both porosity and permeability. This phenomenon is evidenced by a higher proportion of silicon-containing bioclastic limestone samples exhibiting porosity values below 10% and permeability levels under 0.1 mD (Figure 14). Additionally, there is a notable increase in the proportion of samples with porosity values ranging from 10% to 15%. Overall, intense silicification has a destructive effect on reservoir properties, leading to a significant decline in both porosity and permeability. However, moderate silicification, characterized by the formation of

thin siliceous rims around pores, may play a role in isolating and preserving these pores.

5.5 Reservoir formation of lacustrine carbonate rocks

Reservoirs in the Itapema and Barra Velha Formations exhibit significant vertical heterogeneity. Porous and vuggy predominantly develop in the middle to upper parts of sedimentary cycles (Figures 9, 10). This distribution is closely related to the vertical evolution of reservoir rocks and facies sequences driven by high-frequency lake-level fluctuations. Additionally, the properties of the depositional water and syndepositional volcanic activity further influenced the properties of diagenetic pore fluids, thereby

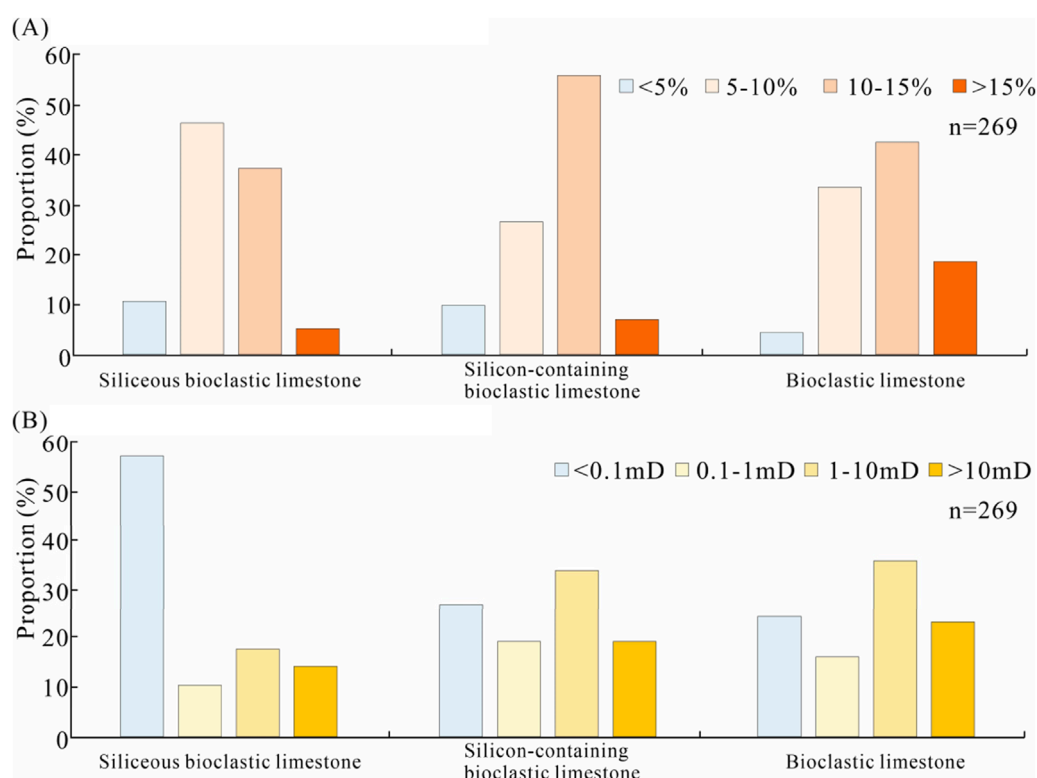


FIGURE 14 Statistical histogram of porosity and permeability of siliceous rocks. (A) Distribution histogram of porosity. (B) Distribution histogram of permeability.

controlling the differential evolution of various of reservoir types (Figures 15, 16).

5.5.1 Formation process of reservoirs of Itapema Formation

Depositional stage: The depositional stage was characterized by the formation of rudstones, which was influenced by hydrodynamic sorting, resulting in the formation of abundant interparticle pores and vugs. In contrast, packstones exhibited reduced porosity due to the extensive infilling of mud within interparticle spaces. Moreover, within sedimentary cycles, there was a progressive enhancement of reservoir quality in an upward direction. Additionally, syn-depositional processes, including submarine cementation and magmatic activity, contributed to the formation of rim-like calcite and siliceous cements (Figure 15), which effectively occluded pore throats and isolated the pores (Figures 2B, E).

Penecontemporaneous to shallow burial stage: The relative decline in lake level during this stage facilitated fabric-selective dissolution of shell fragments, which resulted in the formation of intraparticle dissolved pores or moldic pores (Figure 2E). Prolonged exposure of shoals led to significant dissolution of numerous shell fragments, thereby connecting the pores and creating channels that further increased porosity (Figure 2F). Compared to low-energy deposits located at the base of sedimentary cycles, the shoals at the top of these cycles experienced more significant dissolution, resulting in a more substantial enhancement of porosity. The evolution of reservoir follows a

karstification sequence that progresses from interparticle pores, to interparticle dissolved pores, followed by moldic pores, and lastly culminating in channels. Additionally, the formation of fractures effectively enhance the permeability of low-energy shoals (Figure 10A). The moderate karstification enhances reservoir porosity (Figure 15).

Medium to deep burial Stage: Siliceous fluids have both positive and negative effects on reservoir quality: (1) severe cementation that diminishes pore space and (2) siliceous rim-like cementation that promotes pore preservation (Figure 15). First of all, in terms of damage, calcite and silica cements infill and reduces reservoir space. Reservoir space of low-energy deposits are often completely cemented, leaving only intraparticle dissolved pores or a small number of interparticle pores (Figure 2D). Secondly, in terms of preservation, siliceous rim-like cementation is considered beneficial for preserving pores. In the studied area, these siliceous rim-like cements not only enhance the density of the rocks, thereby increasing its resistance to compaction and freshwater dissolution (Figure 2G), but also inhibit material exchange between pores during the shallow burial stage. This condition establishes a dissolution-precipitation equilibrium, which is conducive to pore preservation (Figure 2B).

5.5.2 Formation process of reservoirs of Barra Velha Formation

Depositional Stage: The primary porosity of the Barra Velha Formation exhibited significant differentiation. The expansion of the growth-framework contributed to enhancements in both porosity

Stage/Setting Diagenetic processes and events	Lacustrine	Penecontemporaneous to shallow burial	Medium to deep burial	Reservoir quality enhanced/reduced (+/-)
Lacustrine carbonate	█			
Micritization	█			+
Hydrothermal fluids migration (Siliceous cementation)	---	---		+
			---	-
Compaction		---	█	-
Fracturing		█		+
Mild-moderate karstification		█		+
Severe karstification		█		-
Dolomitization		█		-
Recrystallization			█	-
Coars calcite cementation			█	-

FIGURE 15 Paragenetic sequence showing various diagenetic phases within the carbonate succession and its relationship with the evolution of petrophysical properties.

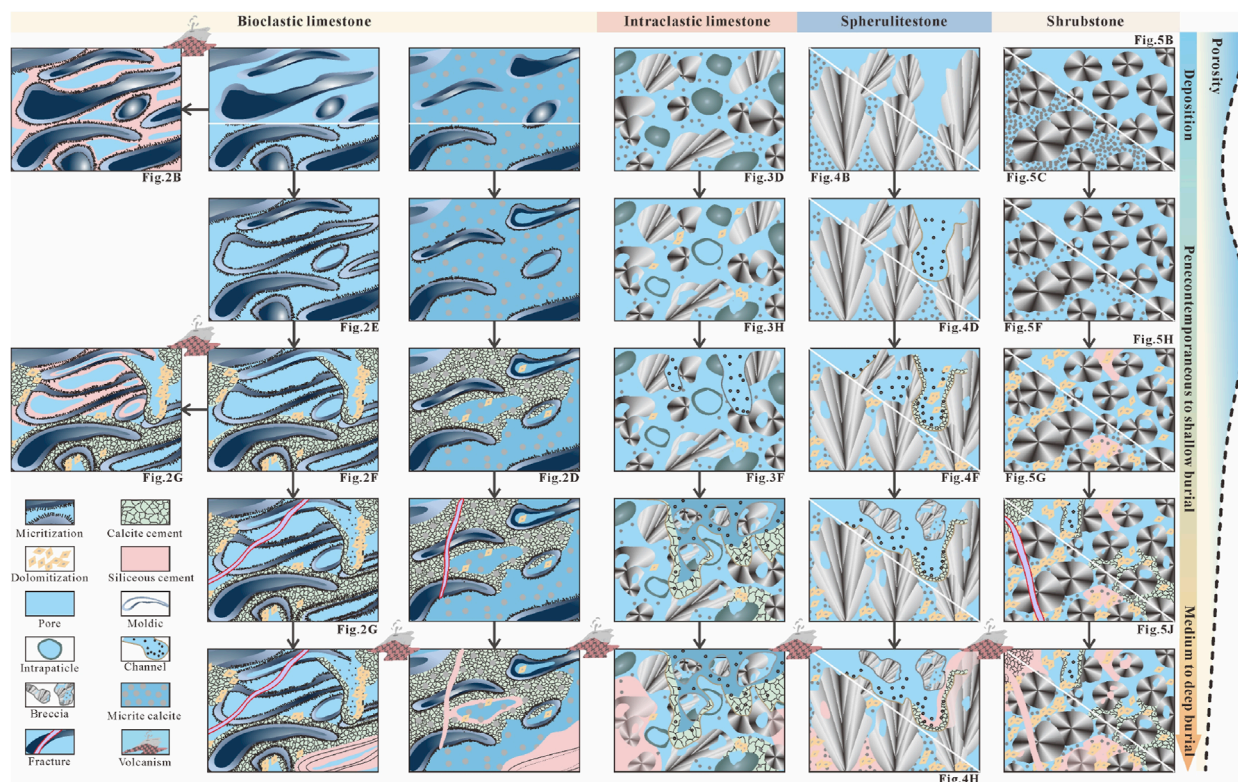


FIGURE 16 Schematic representation of karstification, dolomitization, and cements infilling secondary porosity in this study.

and permeability. Additionally, the interparticle pores within the intraclastic limestone are the high-quality primary reservoir spaces. However, in low-energy environments, the deposition of calcite, mud, and Mg-silicate clays under highly alkaline conditions often infilled the pores, thereby reducing the reservoir quality of the carbonate rocks.

Penecontemporaneous to shallow burial stage: The moderate karstification significantly enhanced reservoir properties (Figure 15). Compared to the Itapema Formation, the Barra Velha Formation exhibits more pronounced degree of karstification process, which has facilitated the formation of various pore types, including intraparticle dissolved pores, interparticle dissolved pores, growth-framework dissolved pores, and intercrystalline dissolved pores. On the other hand, Mg-silicate clays, which exhibit high instability and sensitivity to pH fluctuations, were preferentially destabilized and dissolved during the initial stage of freshwater leaching stage. This dissolution process, occurring between spherulites and growth-frameworks, resulted in the creation of numerous new pores while simultaneously releasing Mg^{2+} and $SiO_2(aq)$ into the lacustrine environment (Tosca and Wright, 2018). The heightened intensity of karstification processes at the top of facies cycles frequently resulted in structural collapse, which subsequently compromised the reservoir properties of shrubstones or intraclastic limestones (Figures 10B, 15). The evolution of reservoir follows a karstification sequence that progresses from interparticle pores or growth-framework pores, to intraparticle dissolved pores, followed by channels, and lastly culminating in breccia. This sequence illustrates a shift in reservoir quality from suboptimal to optimal, and then to a state of degradation (Figure 10B).

Medium to deep burial Stage: The progressive increase in salinity and alkalinity of the lake resulted in the dissolution of Mg^{2+} and $SiO_2(aq)$ which facilitated the precipitation of significant quantities of penecontemporaneous fine-to medium-grained dolomite and quartz within pore spaces (Figure 15), leading to deterioration in reservoir properties (Herlinger et al., 2017; Tosca and Wright, 2018; Lima and De Ros, 2019). This effect was particularly pronounced at the upper section of the Barra Velha Formation, where Late Cretaceous Campanian intrusions (Liu et al., 2023) introduced siliceous hydrothermal fluids that extensively cemented and infilled pores, even leading to the replacement of the carbonate matrix. This process caused significant compaction and densification of the reservoir (Figures 3C, H, I), reducing reservoir quality and contributing to the formation of interbedded sealing layers between high-permeability zones in the studied area (Figure 15).

Despite the formation of numerous pores within the Barra Velha Formation due to dissolution processes, the absence of efficient preservation mechanisms has resulted in a progressive reduction of porosity. This decline is attributed to the synergistic effects of intense dissolution and severe cementation (Figure 16).

6 Conclusion

- (1) In the Cretaceous field A of the Santos Basin, there are well-developed lacustrine carbonate reservoirs. The Itapema Formation primarily made up of bioclastic limestones with

abundant primary interparticle pores, exhibiting relatively favorable porosity and permeability characteristics. These reservoirs are classified as high porosity and high permeability reservoirs. As the properties of the lake water changed, the reservoir rocks in the Barra Velha Formation transformed into shrubstones, intraclastic limestones, and spherulitstones, with reservoir spaces primarily consisting of growth-framework pores and interparticle pores. Overall, the porosity and permeability characteristics have slightly diminished, leading to their classification as medium–high porosity and high permeability or medium porosity and medium–low permeability reservoirs.

- (2) The reservoirs in the studied area exhibit distinct cyclicity, mainly found in the middle to upper parts of upward-shallowing cycles. Overall, reservoir properties improve progressively from the base to the top of these cycles. The stacking of high-frequency sedimentary cycles further enhances the vertical heterogeneity of the reservoirs.
- (3) Fluctuations in lake levels not only facilitated the development of high-frequency cycles but also exposed carbonate reservoirs to penecontemporaneous karstification. Reservoir spaces in the study area were either improved or new types were created, including interparticle dissolved pores, moldic pores, and small cavern. The vertical reservoir evolution within a single cycle follows the progression from primary pores, to intraparticle dissolved pores, followed by channels, and lastly culminating in breccia. Reservoir properties typically improve as one moves with karstification process. However, if karstification intensity is too high at the top of the cycles, it can lead to mud filling in breccia, which diminishes reservoir quality.
- (4) The multiphase magmatic activity associated with rift evolution exerted a dual control on the reservoirs. Significant silicification led to the complete infilling of pores and fractures with siliceous cements, which negatively affected reservoir quality. However, during the synsedimentary stage, quartz preferentially formed rim-like cements along the edges of pores, which often blocked pore throats and caused pore isolation. This process inhibited material exchange between pores during the burial stage, achieving a dissolution-precipitation equilibrium and thereby promoting pore preservation.
- (5) Overall, the reservoirs in the Itapema Formation experienced a progression from excellent primary porosity to karst-enhanced intraparticle pores, and finally leading to rim-like siliceous cementation that preserved the pores. In contrast, the Barra Velha Formation underwent a different reservoir development process from differentiation of matrix porosity, to enhancement of pores due to karstification, followed by the infilling of dolomite and siliceous cements within pores.

Data availability statement

The original contributions presented in the study are included in the article/supplementary material, further inquiries can be directed to the corresponding author.

Author contributions

MY: Writing–original draft, Writing–review and editing. XT: Methodology, Supervision, Writing–review and editing. FX: Writing–review and editing, Resources. DH: Resources, Writing–review and editing. JZ: Resources, Writing–review and editing. CL: Resources, Writing–review and editing. JH: Resources, Writing–review and editing. PL: Writing–review and editing.

Funding

The author(s) declare that no financial support was received for the research and/or publication of this article.

Conflict of interest

Authors MY, XT, and PL were employed by China National Petroleum Corporation.

References

- Alonso–Zarza, A. M., Cabaleri, N. G., Huerta, P., Armella, C., Rodríguez–Berriguete, Á., Monferran, M. D., et al. (2020). Lacustrine microbialite pinnacles in the palaeogene of patagonia, Argentina: facies and controls. *Sediment. Geol.* 408, 105742. doi:10.1016/j.sedgeo.2020.105742
- Andrews, S. D., and Hartley, A. J. (2015). The response of lake margin sedimentary systems to climatically driven lake level fluctuations: middle Devonian, Orcadian Basin, Scotland. *Sedimentology* 62, 1693–1716. doi:10.1111/sed.12200
- Aslanian, D., Moulin, M., Olivet, J.-L., Unternehr, P., Matias, L., Bache, E., et al. (2009). Brazilian and african passive margins of the central segment of the South Atlantic ocean: kinematic constraints. *Tectonophysics* 468 (1–4), 98–112. doi:10.1016/j.tecto.2008.12.016
- Basilone, L., Perri, F., Sulli, A., and Critelli, S. (2017). Paleoclimate and extensional tectonics of short-lived lacustrine environments. Lower Cretaceous of the Panormide Southern Tethyan carbonate platform (NW Sicily). *Mar. Pet. Geol.* 88, 428–439. doi:10.1016/j.marpetgeo.2017.08.041
- Basilone, L., Roberts, G. G., Maia de Almeida, N., Fernandes, V. M., De Souza, A. C. B., Alves, D. P. V., et al. (2024). Cretaceous to recent tectono-sedimentary history and subsidence of the barreirinhas, ceará and potiguar basins, Brazilian equatorial margin. *Basin Res.* 36 (1), e12810. doi:10.1111/bre.12810
- Basso, M., Belila, A. M. P., Chinelatto, G. F., Souza, J. P. D., and Vidal, A. C. (2021). Sedimentology and petrophysical analysis of pre-salt lacustrine carbonate reservoir from the Santos Basin, southeast Brazil. *Int. J. Earth Sci.* 110, 2573–2595. doi:10.1007/s00531-020-01932-7
- Buckley, J. P., Bosence, D., and Elders, C. (2015). Tectonic setting and stratigraphic architecture of an early cretaceous lacustrine carbonate platform, sugar loaf high, Santos Basin, Brazil. *Spec. Publ. – Geol. Soc. Lond.* 418, 175–191. doi:10.1144/SP418.13
- Carvalho, A. M. A., Hamon, Y., De Souza Jr, O. G., Carramal, N. G., and Collard, N. (2022). Facies and diagenesis distribution in an Aptian pre-salt carbonate reservoir of the Santos Basin, offshore Brazil: a Comprehensive Quantitative Approach. *Mar. Pet. Geol.* 141, 105708. doi:10.1016/j.marpetgeo.2022.105708
- Chen, W. F. (2022). *Sedimentary system characteristics of rift strata in the great Campos Basin, eastern Brazil*. Beijing: China University of Petroleum.
- Cheng, T., Kang, H., Liang, J., Jia, H., Bai, B., and Li, M. (2019). Genetic classification and activity periods analysis of magmatic rocks in Santos basin, Brazil. *China Offshore Oil Gas.* 31, 55–66. doi:10.11935/i.issn.1673-1506.2019.04.007
- Chidsey, T. C., Jr., Vanden Berg, M. D., and Eby, D. E. (2015). Petrography and characterization of microbial carbonates and associated facies from modern great salt lake and uinta basin's eocene green river formation in Utah, USA. *Spec. Publ. – Geol. Soc. Lond.* 418, 261–286. doi:10.1144/sp418.6
- Chinelatto, G. F., Belila, A. M. P., Basso, M., Souza, J. P. P., and Vidal, A. C. A. (2020). A taphofacies interpretation of shell concentrations and their relationship with petrophysics: a case study of Barremian–Aptian coquinas in the Itapema Formation, Santos Basin–Brazil. *Mar. Pet. Geol.* 116, 104317. doi:10.1016/j.marpetgeo.2020.104317
- Costa De Oliveira, L., Rancan, C. C., Sartorato, A. C. L., Farias, F. A., and Pereira, E. (2021). Drowning unconformities on presalt carbonate platforms – examples from the Itapema Formation (lower cretaceous), Santos Basin, offshore Brazil. *Palaeogeogr. Palaeoclimatol. Palaeoecol.* 577, 110570. doi:10.1016/j.palaeo.2021.110570
- De Oliveira Nardi Leite, C., De Assis Silva, C. M., and De Ros, L. F. (2020). Depositional and diagenetic processes in the pre-salt rift section of a Santos Basin area, SE Brazil. *Sediment. Res.* 90, 584–608. doi:10.2110/jsr.2020.27
- Einsele, G. (2000). *Sedimentary basins*. Berlin, Heidelberg: Springer Berlin Heidelberg.
- Farias, F., Szatmari, P., Bahniuk, A., and França, A. B. (2019). Evaporitic carbonates in the pre-salt of Santos Basin – genesis and tectonic implications. *Mar. Pet. Geol.* 105, 251–272. doi:10.1016/j.marpetgeo.2019.04.020
- Ghafor, I. M. (2022). “Biostratigraphy and microfacies of azkand formation in qarrah chugh-dagh section, kirkuk area (northeastern Iraq),” in *Recent research on geomorphology, sedimentology, marine geosciences and geochemistry: proceedings of the 2nd springer conference of the arabian journal of geosciences (CAJG-2), Tunisia 2019* (Springer International Publishing), 251–256.
- Ghafor, I. M., and Najaflo, S. (2022). Biostratigraphy, microfacies, paleoenvironment, and paleoecological study of the oligocene (late rupelian–early chattian) baba formation, kirkuk area, northeastern Iraq. *Carbonates Evaporites* 37 (1), 7–15. doi:10.1007/s13146-021-00753-2
- Gomes, J. P. B., Bunevich, R. B., Tonietto, S. N., Alves, D. B., Santos, J. F., and Whitaker, F. F. (2020). Climatic signals in lacustrine deposits of the Upper Yacoraité Formation, Western Argentina: evidence from clay minerals, analcime, dolomite and fibrous calcite. *Sedimentology* 67, 2282–2309. doi:10.1111/sed.12700
- Grimes, K. G. (2006). Syngenetic karst in Australia: a review. *Helictite* 39, 27–38.
- He, W., Shi, B., Fang, G., Wang, W., Wang, H., Wang, J., et al. (2023). Theoretical and technical progress in exploration practice of the deep-water large oil fields, Santos Basin, Brazil. *Petrol. explor. Dev.* 50, 255–267. doi:10.1016/S1876-3804(22)60385-9
- Herlinger, R., Zambonato, E. E., and De Ros, L. F. (2017). Influence of diagenesis on the quality of lower cretaceous pre-salt lacustrine carbonate reservoirs from northern Campos Basin, offshore Brazil. *Sediment. Res.* 87, 1285–1313. doi:10.2110/jsr.2017.70
- Jia, H., Kang, H., Liang, J., Cheng, T., and Zhang, S. (2021). Characteristic and developmental controlled factors of pre-salt lacustrine carbonate, Santos Basin. *J. Southwest Pet. Univ. Sci. Technol.* 43, 1–9. doi:10.11885/j.issn.1674-5086.2019.07.18.02
- Keller, G. (2008). Cretaceous climate, volcanism, impacts, and biotic effects. *Cretac. Res.* 29, 754–771. doi:10.1016/j.cretres.2008.05.030
- Leleu, S., and Hartley, A. (2010). Controls on the stratigraphic development of the triassic fundy basin, nova scotia: implications for the tectonostratigraphic evolution of triassic atlantic rift basins. *Geol. Soc. Lond.* 167, 437–454. doi:10.1144/0016-76492009-092

- Li, F., Yan, J., Chen, Z., Ogg, J. G., Tian, L., Korngreen, D., et al. (2015). Global oolite deposits across the Permian–Triassic boundary: a synthesis and implications for palaeoceanography immediately after the end–Permian biocrisis. *Earth–Sci. Rev.* 149, 163–180. doi:10.1016/j.earscirev.2014.12.006
- Li, H., Li, F., Li, X., Zeng, K., Gong, Q., Yi, C., et al. (2021). Development and collapse of the Early Cambrian shallow–water carbonate factories in the Hannan–Micangshan area, south China. *Palaeogeogr. Palaeoclimatol. Palaeoecol.* 583, 110665. doi:10.1016/j.palaeo.2021.110665
- Li, L., Xiao, D., Liu, R., Zhang, Y., Shan, S., Liu, Y., et al. (2023). Origin of breccia dolomites in the middle devonian guanwushan formation, NW sichuan basin, China: implications for ultra–deepcarbonate reservoirs. *Geoenergy Sci. Eng.* 227, 211949. doi:10.1016/j.geoen.2023.211949
- Lima, B. E. M., and De Ros, L. F. (2019). Deposition, diagenetic and hydrothermal processes in the Aptian pre–salt lacustrine carbonate reservoirs of the northern Campos Basin, offshore Brazil. *Sediment. Geol.* 383, 55–81. doi:10.1016/j.sedgeo.2019.01.006
- Lima, B. E. M., Tedeschi, L. R., Pestilho, A. L. S., Santos, R. V., Vazquez, J. C., Guzzo, J. V. P., et al. (2020). Deep–burial hydrothermal alteration of the pre–salt carbonate reservoirs from northern Campos Basin, offshore Brazil: evidence from petrography, fluid inclusions, Sr, C and O isotopes. *Mar. Pet. Geol.* 113, 104143. doi:10.1016/j.marpetgeo.2019.104143
- Liu, Y., Wang, D., Tian, Z., Zhang, Z., Wang, T., Wang, C., et al. (2023). Characteristics and prediction methods of igneous rocks in complex carbonate oilfields in Santos Basin, Brazil. *Lithol. Reserv.* 35, 127–137. doi:10.12108/xyqy.20230614
- McArthur, A. D., Hartley, A. J., and Jolley, D. W. (2013). Stratigraphic development of an upper jurassic deep marine syn–rift succession, inner moray firth basin, scotland. *Basin Res.* 25 (3), 285–309. doi:10.1111/j.1365-2117.2012.00557.x
- Mehrabi, H., Mansouri, M., Rahimpour–Bonab, H., Tavakoli, V., and Hassanzadeh, M. (2016). Chemical compaction features as potential barriers in the Permian–Triassic reservoirs of Southern Iran. *J. Pet. Sci. Eng.* 145, 95–113. doi:10.1016/j.petrol.2016.03.020
- Mehrabi, H., Ranjbar–Karami, R., and Roshani–Nejad, M. (2019). Reservoir rock typing and zonation in sequence stratigraphic framework of the Cretaceous Dariyan Formation, Persian Gulf. *Carbonates Evaporites* 34, 1833–1853. doi:10.1007/s13146-019-00530-2
- Mercedes–Martín, R., Ayora, C., Tritlla, J., and Sánchez–Román, M. (2019). The hydrochemical evolution of alkaline volcanic lakes: a model to understand the South Atlantic pre–salt mineral assemblages. *Earth–Sci. Rev.* 198, 102938. doi:10.1016/j.earscirev.2019.102938
- Mercedes–Martín, R., Rao, A., Rogerson, M., and Sánchez–Román, M. (2022). Effects of salinity, organic acids and alkalinity on the growth of calcite spherulites: implications for evaporitic lacustrine sedimentation. *Depos. Rec.* 8 (1), 143–164. doi:10.1002/dep2.136
- Mizusaki, A. M. P., Petrini, R., Bellieni, G., Comin–Chiaromonte, P., Dias, J., De Min, A., et al. (1992). Basalt magmatism along the passive continental margin of SE Brazil (Campos basin). *Mineral. Petrol.* 111, 143–160. doi:10.1007/bf00348948
- Modica, C. J., and Brush, E. R. (2004). Postrift sequence stratigraphy, paleogeography, and fill history of the deep–water Santos Basin, offshore southeast Brazil. *AAPG Bull.* 88, 923–945. doi:10.1306/01220403043
- Moore, C. H., and Wade, W. J. (2013). “Carbonate reservoirs: porosity and diagenesis in a sequence stratigraphic framework,” in *Developments in sedimentology*. Second edition (Amsterdam: Elsevier).
- Moreira, J. L. P., Madeira, C. V., Gil, J. A., and Machado, M. A. P. (2007). Bacia de Santos. *Bol. Geociências Petrobras* 15, 531–549.
- Moulin, M., Aslanian, D., and Unternehr, P. (2010). A new starting point for the South and equatorial atlantic ocean. *Earth–Sci. Rev.* 98 (1–2), 1–37. doi:10.1016/j.earscirev.2009.08.001
- Murphy, D. H., and Wilkinson, B. H. (1980). Carbonate deposition and facies distribution in a central Michigan marl lake. *Sedimentology* 27, 123–135. doi:10.1111/j.1365-3091.1980.tb01164.x
- O’Connor, J. M., and Duncan, R. A. (1990). Evolution of the Walvis Ridge–Rio Grande Rise hot spot system: implications for african and south American plate motions over plumes. *J. Geophys. Res.* 95, 17475–17502. doi:10.1029/JB095iB11p17475
- Pietzsch, R., Oliveira, D. M., Tedeschi, L. R., Queiroz Neto, J. V., Figueiredo, M. F., Vazquez, J. C., et al. (2018). Palaeohydrology of the Lower Cretaceous pre–salt lacustrine system, from rift to post–rift phase, Santos Basin, Brazil. *Palaeogeogr. Palaeoclimatol. Palaeoecol.* 507, 60–80. doi:10.1016/j.palaeo.2018.06.043
- Pietzsch, R., Tedeschi, L. R., Oliveira, D. M., Dos Anjos, C. W. D., Vazquez, J. C., and Figueiredo, M. F. (2020). Environmental conditions of deposition of the Lower Cretaceous lacustrine carbonates of the Barra Velha Formation, Santos Basin (Brazil), based on stable carbon and oxygen isotopes: a continental record of pCO₂ during the onset of the Oceanic Anoxic Event 1a (OAE 1a) interval? *Chem. Geol.* 535, 119457. doi:10.1016/j.chemgeo.2019.119457
- Pietzsch, R., Tosca, N. J., Gomes, J. P., Roest–Ellis, S., Sartorato, A. C. L., and Tonietto, S. N. (2022). The role of phosphate on non–skeletal carbonate production in a Cretaceous alkaline lake. *Geochim. Cosmochim. Acta* 317, 365–394. doi:10.1016/j.gca.2021.09.032
- Pomar, L., and Hallock, P. (2008). Carbonate factories: a conundrum in sedimentary geology. *Earth–Sci. Rev.* 87 (3–4), 134–169. doi:10.1016/j.earscirev.2007.12.002
- Poropat, S. F., and Colin, J.–P. (2012a). Reassessment of the Early Cretaceous non–marine ostracod genera *Hourcquia* Krömmelbein, 1965 and *Pattersoncypris* Bate, 1972 with the description of a new genus, *Kroemmelbeincypris*. *J. Paleontol.* 86 (4), 699–719. doi:10.1666/11-140R.1
- Poropat, S. F., and Colin, J.–P. (2012b). Early Cretaceous ostracod biostratigraphy of eastern Brazil and western Africa: an overview. *Gondwana Rese* 22 (3–4), 772–798. doi:10.1016/j.gr.2012.06.002
- Read, J. F. (1982). Carbonate platforms of passive (extensional) continental margins: types, characteristics and evolution. *Tectonophysics* 81 (3), 195–212. doi:10.1016/0040-1951(82)90129-9
- Read, J. F. (1985). Carbonate platform facies models. *AAPG Bull.* 69 (1), 1–21. doi:10.1306/AD461B79-16F7-11D7-8645000102C1865D
- Rebello, T. B., Batezelli, A., and Luna, J. S. (2021). Stratigraphic evolution and carbonate factory implications: case study of the Albian carbonates of the Campos Basin, Brazil. *Depositional Rec.* 7, 271–293. doi:10.1002/dep2.118
- Reijmer, J. J. G. (2021). Marine carbonate factories: review and update. *Sedimentology* 68, 1729–1796. doi:10.1111/sed.12878
- Rodriguez, C. R., Jackson, C. A. L., Rotevatn, A., Bell, R. E., and Francis, M. (2018). Dual tectonic–climatic controls on salt giant deposition in the Santos Basin, offshore Brazil. *Geosphere* 14, 215–242. doi:10.1130/GES01434.1
- Saller, A., Rushton, S., Buambua, L., Inman, K., McNeil, R., and Dickson, J. T. (2016). Presalt stratigraphy and depositional systems in the Kwana Basin, offshore Angola. *AAPG Bull.* 100, 1135–1164. doi:10.1306/02111615216
- Saller, A. H., Dickson, J. A. D., and Matsuda, F. (1999). Evolution and distribution of porosity associated with subaerial exposure in upper Paleozoic platform limestones, west Texas. *AAPG Bull.* 83, 1835–1854. doi:10.1306/E4FD4279-1732-11D7-8645000102C1865D
- Schlager, W. (2003). Benthic carbonate factories of the Phanerozoic. *Int. J. Earth Sci.* 92, 445–464. doi:10.1007/s00531-003-0327-x
- Schlager, W. (2005). *Carbonate sedimentology and sequence stratigraphy*. Tulsa: SEPM, 1–208.
- Scotchman, I. C., Gilchrist, G., Kuszniir, N. J., Roberts, A. M., and Fletcher, R. (2010). The breakup of the South Atlantic Ocean: formation of failed spreading axes and blocks of thinned continental crust in the Santos Basin, Brazil and its consequences for petroleum system development. *Pet. Geol. Conf. Ser.* 7, 855–866. doi:10.1144/0070855
- Shah, M. M., Afridi, S., Khan, E. U., Rahim, H. U., and Mustafa, M. R. (2021). Diagenetic modifications and reservoir heterogeneity associated with magmatic intrusions in the devonian khyber limestone, peshawar basin, NW Pakistan. *Geofluids* 2021, 1–18. doi:10.1155/2021/8816465
- Shang, Z., Wu, J., Shang, F., Yu, B., Ma, X., Oin, T., et al. (2020). Silicification geneses and their effects on pre–salt carbonate reservoir in M Oilfield, Brazil Santos Basin. *Pet. Geol. Recovery Effic.* 27, 20–29. doi:10.13673/j.cnki.cn37-1359/te.2020.06.003
- Shi, B., Fan, G., Zhao, D., Wang, H., Zhao, J., Liu, Y., et al. (2021). Discussion on the division of subsalt tectonic units of Santos Basin, offshore Brazil. *Mar. Orig. Pet. Geol.* 26, 263–271. doi:10.3969/i.issn.1672-9854.2021.03.008
- Silva Adriano, M., Figueiredo, J. P., Coelho, P. H. G. R., and Borghi, L. (2022). Tectonic and stratigraphic evolution of the Santos Basin rift phase: new insights from seismic interpretation on Tupi oil field area. *J. South Am. Earth Sci.* 116, 103842. doi:10.1016/j.jsames.2022.103842
- Szatmari, P., and Milani, E. J. (2016). Tectonic control of the oil–rich large igneous–carbonate–salt province of the South Atlantic rift. *Mar. Pet. Geol.* 77, 567–596. doi:10.1016/j.marpetgeo.2016.06.004
- Thompson, D. L., Stilwell, J. D., and Hall, M. (2015). Lacustrine carbonate reservoirs from Early Cretaceous rift lakes of western gondwana: pre–salt coquinas of Brazil and west Africa. *Gondwana Rese* 28, 26–51. doi:10.1016/j.gr.2014.12.005
- Torsvik, T. H., Rouse, S., Labails, C., and Smethurst, M. A. (2009). A new scheme for the opening of the South Atlantic ocean and the dissection of an aptian salt basin. *Geophys. J. Int.* 177, 1315–1333. doi:10.1111/j.1365-246X.2009.04137.x
- Tosca, N. J., and Wright, V. P. (2018). Diagenetic pathways linked to labile Mg–clays in lacustrine carbonate reservoirs: a model for the origin of secondary porosity in the Cretaceous pre–salt Barra Velha Formation, offshore Brazil. *Spec. Publ. – Geol. Soc. Lond.* 435, 33–46. doi:10.1144/SP435.1
- Tucker, M. E., Wright, V. P., and Dickson, J. A. D. (1990). *Carbonate sedimentology*. Oxford: Blackwell Science Publications, 1–482. doi:10.1002/9781444314175
- Wei, W., Azmy, K., and Zhu, X. (2022). Impact of diagenesis on reservoir quality of the lacustrine mixed carbonate–siliciclastic–volcaniclastic rocks in China. *J. Asian Earth Sci.* 233, 105265. doi:10.1016/j.jseas.2022.105265
- Wright, V. P. (2012). Lacustrine carbonates in rift settings: the interaction of volcanic and microbial processes on carbonate deposition. *Spec. Publ. – Geol. Soc. Lond.* 370 (1), 39–47. doi:10.1144/SP370.2

- Wright, V. P. (2022). The mantle, CO₂ and the giant Aptian chemogenic lacustrine carbonate factory of the South Atlantic: some carbonates are made, not born. *Sedimentology* 69, 47–73. doi:10.1111/sed.12835
- Wright, V. P., and Barnett, A. J. (2015). An abiotic model for the development of textures in some South Atlantic early Cretaceous lacustrine carbonates. *Spec. Publ. – Geol. Soc. Lond.* 418 (1), 209–219. doi:10.1144/SP418.3
- Wright, V. P., and Barnett, A. J. (2020). The textural evolution and ghost matrices of the Cretaceous Barra Velha Formation carbonates from the Santos Basin, offshore Brazil. *Facies* 66, 7. doi:10.1007/s10347-019-0591-2
- Wu, K., Xiong, Y., Tan, X., Liu, X., Zhang, Y., Chen, X., et al. (2022). Study of the crystallization kinetics for “water-rock” interactions in the reservoir pore-system: an overview. *Acta Sedimentol. Sin.* 40, 996–1009. doi:10.14027/j.issn.1000-0550.2021.029
- Xiao, D., Cao, J., Tan, X., Xiong, Y., Zhang, D., Dong, G., et al. (2021). Marine carbonate reservoirs formed in evaporite sequences in sedimentary basins: a review and new model of epeiric basin-scale moldic reservoirs. *Earth-Sci. Rev.* 223, 103860. doi:10.1016/j.earscirev.2021.103860
- Xiao, D., Tan, X., Xi, A., Liu, H., Shan, S., Xia, J., et al. (2016). An inland facies-controlled eogenetic karst of the carbonate reservoir in the Middle Permian Maokou Formation, southern Sichuan Basin, SW China. *Mar. Pet. Geol.* 72, 218–233. doi:10.1016/j.marpetgeo.2016.02.001
- Xie, K., Tan, X., Feng, M., Wang, B., Zhong, S., Yang, M., et al. (2020). Eogenetic karst and its control on reservoirs in the ordovician majiagou formation, eastern sulige gas field, ordos basin, NW China. *Petrol. explor. Dev.* 47, 1246–1261. doi:10.1016/S1876-3804(20)60133-7
- Xiong, L., Xie, X., Deng, Y., Tang, W., Zhang, C., Bai, H., et al. (2023b). Genesis and evolution of Lower Cretaceous silicified carbonate reservoirs in southern Campos Basin. *Acta Pet. Sin.* 44, 1612–1623. doi:10.7623/syxb202310003
- Xiong, Y., Tan, X., Dong, G., Wang, L., Ji, H., Liu, Y., et al. (2020a). Diagenetic differentiation in the ordovician majiagou formation, ordos basin, China: facies, geochemical and reservoir heterogeneity constraints. *J. Pet. Sci. Eng.* 191, 107179. doi:10.1016/j.petrol.2020.107179
- Xiong, Y., Tan, X., Liu, B., Hou, Z., Luo, J., Wu, L., et al. (2023a). On the dissolution paths and formation mechanisms of paleokarst reservoirs: constraints from reactive transport modeling. *Mar. Pet. Geol.* 156, 106462. doi:10.1016/j.marpetgeo.2023.106462
- Xiong, Y., Tan, X., Wu, K., and Wang, X. (2020b). Research advances, geological implication and application in Ordos Basin of the pore-size controlled precipitation in diagenesis of carbonate rock reservoir. *J. Palaeogeogr. Chin.* 22, 744–760. doi:10.7605/gdxb.2020.04.050
- Xiong, Y., Tan, X., Wu, K., Xu, Q., Liu, Y., and Qiao, Y. (2021). Petrogenesis of the Eocene lacustrine evaporites in the western Qaidam Basin: implications for regional tectonic and climate changes. *Sediment. Geol.* 416, 105867. doi:10.1016/j.sedgeo.2021.105867
- Xiong, Y., Tan, X., Zhong, S., Xiao, D., Wang, B., Yang, M., et al. (2022). Dynamic paleokarst geochemistry within 130 Myr in the middle ordovician shanganning carbonate platform, north China. *Palaeogeogr. Palaeoclimatol. Palaeoecol.* 591, 110879. doi:10.1016/j.palaeo.2022.110879
- Xiong, Y., Tan, X., Zuo, Z., Zou, G., Liu, M., Liu, Y., et al. (2019). Middle Ordovician multi-stage pencontemporaneous karstification in North China: implications for Reservoir genesis and sea level fluctuations. *J. Asian Earth Sci.* 183, 103969. doi:10.1016/j.jseae.2019.103969
- Yang, Y., Liang, C., Liu, F., Li, Y., Zhang, L., Sun, H., et al. (2024). Predicting carbonate rock dissolution using multi-scale residual neural networks with prior knowledge. *Gas. Sci. Eng.* 124, 205268. doi:10.1016/j.jgsce.2024.205268
- Ye, Y., Li, F., Song, X., and Gou, R. (2021). Transformation mechanism of argillaceous carbonate rock by the coupling of bioturbation and diagenesis: a case study of the Cretaceous System of the Mesopotamia Basin in the Middle East. *Petrol. explor. Dev.* 48, 1187–1201. doi:10.1016/S1876-3804(21)60293-8
- Yuretich, R. F., and Cerling, T. E. (1983). Hydrogeochemistry of Lake Turkana, Kenya: mass balance and mineral reactions in an alkaline lake. *Geochim. Cosmochim. Acta* 47, 1099–1109. doi:10.1016/0016-7037(83)90240-5
- Zhang, Z., Zhu, Y., Zhang, D., Su, Y., Yao, W., Bao, Z., et al. (2020). Hydrocarbon accumulation rules and exploration inspiration of pre-salt carbonate reservoirs in the Great Campos Basin, Brazil. *China Pet. Explor* 25, 75–85. doi:10.3969/i.issn.1672-7703.2020.04.008
- Zhao, L., Zhou, W., Zhong, Y., Gou, R., Jin, M., and Chen, Y. (2019). Control factors of reservoir oil-bearing difference of Cretaceous Mishrif Formation in the H oilfield, Iraq. *Petrol. explor. Dev.* 46, 314–323. doi:10.1016/S1876-3804(19)60011-X
- Zhong, Y., Tan, X., Zhao, L., Guo, R., Li, F., Jin, Z., et al. (2019). Identification of facies-controlled eogenetic karstification in the Upper Cretaceous of the Halfaya oilfield and its impact on reservoir capacity. *Geol. J.* 54, 450–465. doi:10.1002/gj.3193